Semiannual Technical Report

Growth and Doping of $Al_xGa_{1-x}N$ Films by Electron Cyclotron Resonance Assisted Molecular Beam Epitaxy

ONR Grant No. N00014-92-J-1436
(May 1, 1993 – October 30, 1993)

P.I. Theodore D. Moustakas

Department of Electrical,
Computer and Systems Engineering

Boston University
Boston, MA 02215
617-353-5431

November 30, 1993

REPORT DOCUMENTATION PAGE

Form Approved
OMB No 0704-0188

1. AGENCY USE ONLY (Leave Blank)	2. REPORT DATE	3. REPORT TYPE AND DATES COVERED
	30Nov93	Annual 01May93 - 30Oct93

4. TITLE AND SUBTITLE
Growth and Doping of $Al_xGa_{1-x}N$ Films by Electron Cyclotron Resonance Assisted Molecular Beam Epitaxy

5. FUNDING NUMBERS
R&T: 4145329---01
S.O: 1114SS
AGO: N66017
CAGE: 3A817

6. AUTHOR(S)
Moustakas, Theodore D.

7. PERFORMING ORGANIZATION NAME(S) AND ADDRESS(ES)
Boston University
College of Engineering
44 Cummington St.
Boston, MA 02215

8. PERFORMING ORGANIZATION REPORT NUMBER
N00014-92-J-1436

9. SPONSORING/MONITORING AGENCY NAME(S) AND ADDRESS(ES)
Department of the Navy
Office of the Chief of Naval Research
800 North Quincy St.
Arlington, VA 22217-5000

10. SPONSORING/MONITORING AGENCY REPORT NUMBER

11. SUPPLEMENTARY NOTES

12a. DISTRIBUTION/AVAILABILITY STATEMENT
Approved for Public Release; Distribution Unlimited

12b. DISTRIBUTION CODE

13. ABSTRACT *(Maximum 200 words)*

During this funding period the work focused on understanding the origin of defects in GaN grown by the ECR-MBE method and studied their role transport, optical and recombination properties. More specifically from EPR studies we deduced the effective mass of the zincblende structure of GaN to be $m^*=0.15\ m_o$. Photoluminescence studies indicate that the concentration of defect states at 2.2eV is higher on films grown at higher microwave power. The role of hydrogen in the de-activation of p-type doping was investigated by introducing hydrogen in Mg-doped films after their growth. The doping activity is restored upon annealing the hydrogen. TEM studies of GaN film grown on Silicon was completed and reveal that the majority of defects are stacking faults, microtwins and localized regions having the wurtzite structure. In the device area we investigate the RIE of GaN in various reactive gases.

14. SUBJECT TERMS
Gallium Nitride, Molecular Beam Epitaxy, Electron Cyclotron Resonance, defects, hydrogen, TEM, EPR, RIE

15. NUMBER OF PAGES

16. PRICE CODE

17. SECURITY CLASSIFICATION OF REPORT	18. SECURITY CLASSIFICATION OF THIS PAGE	19. SECURITY CLASSIFICATION OF ABSTRACT	20. LIMITATION OF ABSTRACT
UNCLAS	UNCLAS	UNCLAS	

Contents

Appendix A: "Conduction-electron spin resonance in zinc-blende GaN thin films"
Appendix B: "Intensity dependence of photoluminescence in GaN thin films"
Appendix C: "Microstructures of GaN Films Deposited on (001) and (111) Si Using ECR-MBE"
Appendix D: "Hydrogenation of Gallium Nitride"
Appendix E: "Reactive Ion Etching of GaN Thin Films"

1 Summary of results during the funding period

During the funding period we investigated the following topics:

1.1 Conduction-electron spin resonance in zinc-blende GaN thin films

We report electron-spin-resonance measurements on zinc-blende GaN. The observed resonance has and isotropic g value of 1.9533 ± 0.0008 independent of temperature, a Lorentzian line shape, and a linewidth (18 G at 10 K) which depends on temperature. The spin-lattice relaxation time at 10 K was estimated to be $T_{1e} = (6 \pm 2) \times 10^{-5}$ sec. Using a five-band model a g value consistent with the experimental results was obtained and a conduction-electron effective mass $m^*/m_0 = 0.15 \pm 0.014$ was calculated. The observed signal, together with conductivity data, was attributed to nonlocalized electrons in a band of autodoping centers and in the conduction band. For more details see Appendix A.

1.2 Intensity dependence of photoluminescence in GaN thin films

We report the intensity dependence of band-gap and midgap photoluminescence in GaN films grown by electron cyclotron resonance (ECR) microwave plasma-assisted molecular beam epitaxy. We find that the band-gap luminescence depends linearly while the midgap luminescence has a nonlinear dependence on the incident light intensity. These date were compared with a simple recombination model which assumes a density of recombination centers 2.2 eV below the conduction band edge. The concentration of these centers is higher in films grown at higher microwave power in the ECR plasma. For more details see Appendix B.

1.3 Microstructures of GaN Films Deposited on (001) and (111) Si Using ECR-MBE

The microstructures of GaN films, grown on (001) and (111) Si substrates, by a two-step method using ECR-MBE, were studied by electron microscopy techniques. Films grown on (001) Si had a predominantly zinc-blende structure. The GaN buffer layer, grown in the first deposition step accommodated the 17% lattice mismatch between the film and substrate by a combination of misoriented domains and misfit dislocations. Beyond the buffer layer, the film consisted of highly oriented domains separated by inversion domain boundaries, with a substantial decrease in the defect density away from the interface. The majority of defects in the film were stacking faults, microtwins and localized regions having the wurtzitic structure. The structure of the GaN films grown on (111) Si was found to be primarily wurtzitic, with a substantial fraction of twinned zinc-blende phase. Occasional wurtzitic grains, misoriented by a 30° twist along the [0001] axis were also observed. For more details see Appendix C.

1.4 Hydrogenation of Gallium Nitride

A comparative study of the effects of hydrogen in n-type (unintentionally and Si-doped) as well as p-type (Mg-doped) MBE-grown GaN is presented. Hydrogenation above 500°C reduces the hole concentration at room temperature in the p-type material by one order of magnitude. Three different microscopic effects of hydrogen are suggested: Passivation of deep defects and of Mg-acceptors due to formation of hydrogen-related complexes and the introduction of a hydrogen-related donor state 100 meV below the conduction band edge. For more details see Appendix D.

1.5 Reactive Ion Etching of GaN Thin Films

Reactive ion etching of GaN grown by electron-cyclotron-resonance, microwave plasma-assisted molecular beam epitaxy on (0001) sapphire substrates was investigated. A variety of reactive and inert gases such as CCl_2F_2, SF_6, CF_4, H_2/CH_4 mixtures, CF_3Br, CF_3Br/Argon mixtures and Ar were investigated. From these studies we conclude that of the halogen radicals investigated, Cl and Br etch GaN more effectively than F. The etching rate was found to increase with decreasing pressure at a constant cathode voltage, a result attributed to larger mean free path of the reactive species. For more details see Appendix E.

2 Publication List

"Conduction Electron Spin Resonance in Zinc-blende GaN Thin Films"
M. Fanciulli, T. Lei and T.D. Moustakas
Phys. Rev. B, 48, 15144 (1993)
Appendix A

"Intensity Dependence of Photoluminescence in Gallium Nitride Thin Films"
R. Singh, R.J. Molnar, M.S. Ünlü and T.D. Moustakas
Appl. Phys. Lett., 64, 336 (1994)
it Appendix B

"Microstructures of GaN Films Deposited on (001) and (111) Si
Using ECR-MBE"
S.N. Basu, T. Lei and T.D. Moustakas
J. Mater. Res. (submitted)
Appendix C

"Hydrogenation of Gallium Nitride"
M.S. Brandt, N.M. Johnson, R. Molnar, R. Singh and T.D. Moustakas
Mat. Res. Soc. Symp. Proc., accepted (1994)
Appendix D

"Reactive Ion Etching of GaN Thin Films"
M.J. Manfra, S.J. Berkowitz, R.J. Molnar, A.M. Clark, T.D. Moustakas and W.J. Skocpol
Mat. Res. Soc. Symp. Proc., accepted (1994)
Appendix E

"Heteroepitaxy, Polymorphism and Faulting in GaN Thin Films on Silicon and
Sapphire Substrates"
T. Lei, K.F. Ludwid and T.D. Moustakas
J. Appl. Phys., 74, 4430 (1993).

Appendix A:

Conduction-electron spin resonance in zinc-blende GaN Thin Films
Published in *Physical Review B* **48**, 15144 (1993).

Conduction-electron spin resonance in zinc-blende GaN thin films

M. Fanciulli and T. Lei
Department of Physics, Boston University, Boston, Massachusetts 02215

T. D. Moustakas
Department of Physics and Department of Electrical, Computer and Systems Engineering, Boston University, Boston, Massachusetts 02215

(Received 8 July 1993)

We report electron-spin-resonance measurements on zinc-blende GaN. The observed resonance has an isotropic g value of 1.9533 ± 0.0008 independent of temperature, a Lorentzian line shape, and a linewidth (18 G at 10 K) which depends on temperature. The spin-lattice relaxation time at 10 K was estimated to be $T_{1e}=(6\pm2)\times10^{-5}$ sec. Using a five-band model a g value consistent with the experimental results was obtained and a conduction-electron effective mass $m^*/m_0=0.15\pm0.01$ was calculated. The observed signal, together with conductivity data, was attributed to nonlocalized electrons in a band of autodoping centers and in the conduction band.

I. INTRODUCTION

Gallium nitride is a wide-band-gap semiconductor which is anticipated to find applications for optical devices (light-emitting diodes, lasers, detectors) in the near uv region of the electromagnetic spectrum and electronic devices for high-power, high-frequency, and high-temperature applications. GaN was found to exist in two allotropic forms. The wurtzite structure is the thermodynamically stable phase and has an optical gap of 3.5 eV,[1,2] while the zinc-blende structure is a metastable phase which can be formed by epitaxial stabilization[3,4] and has an optical gap of 3.2 eV.[4] In both cases the material is found to be heavily autodoped n type, a result attributed to nitrogen vacancies.[5] In general, the electron concentration is in the range of $10^{17}-10^{20}$ cm^{-3}.

In this paper we report electron-spin-resonance (ESR) studies in autodoped n-type zinc-blende GaN thin films. The data were correlated with electrical conductivity measurements and from their analysis the nature of the resonance was determined. The measured g value was found to be in agreement with theoretical predictions based on a five-band model $\mathbf{k}\cdot\mathbf{p}$ calculation. The same calculation was also used to predict the electron effective mass.

II. EXPERIMENTAL RESULTS AND DISCUSSION

The GaN films were grown by electron-cyclotron-resonance microwave plasma-assisted molecular-beam-epitaxy (MBE). Epitaxial stabilization of the zinc-blende structure was accomplished by using a two-temperature step process on Si(100). In this process a 200-Å GaN buffer was grown at 400 °C and the rest of the film, 4 μm thick, was grown at 600 °C. Both heavily autodoped and semi-insulating GaN films were fabricated and investigated. Transport studies in these films[6] show that the conductivity is dominated by the high-quality top layer rather than by the GaN buffer. Details on the growth are given elsewhere.[3,4] Structural studies (reflection high-energy electron diffraction, electron diffraction, and x-ray diffraction) show that the films are single crystals having the zinc-blende structure with lattice constant 4.5 Å.[3,4]

To conduct optical, transport, and spin-resonance measurements, self-standing GaN flakes were obtained by dissolving the Si substrate with a solution of HNO_3 and HF. The optical gap of the films was determined by transmission measurements and found to be 3.2 eV.[4] The electrical conductivity of one of the investigated films, determined by four probe measurements using sputtered Al contacts, is shown as a function of $1/T$ in Fig. 1. The data fit the expression

$$\sigma=\sigma_1\exp(-\varepsilon_1/kT)+\sigma_3\exp(-\varepsilon_3/kT)\,, \tag{1}$$

where the activation energies ε_1 and ε_3 are 25 and 0.5 meV, respectively.

Hall-effect measurements show that the films are n type; however, we were unable to perform accurate measurements of the carrier concentration on these self-standing GaN flakes. Based on our studies of wurtzite GaN films,[6] we anticipate that the investigated films have room-temperature carrier concentration of the order of $10^{17}-10^{18}$ cm^{-3}. The data of Fig. 1 are consistent with transport in the conduction band at temperatures higher than about 50 K and transport in a band of shallow donors at lower temperatures.[7]

The nature of these shallow donors is still controversial. They have been observed in GaN films produced by various deposition methods and attributed by early workers to nitrogen vacancies.[5] Our thin-film growth studies support this hypothesis. Since our films are grown at temperatures below the decomposition temperature of GaN, their stoichiometry can be controlled by varying the nitrogen overpressure during growth. At low active nitrogen overpressure we find that the films are n type with carrier concentration between $10^{18}-10^{20}$ cm^{-3}. Such films tend also to be decorated with gallium drop-

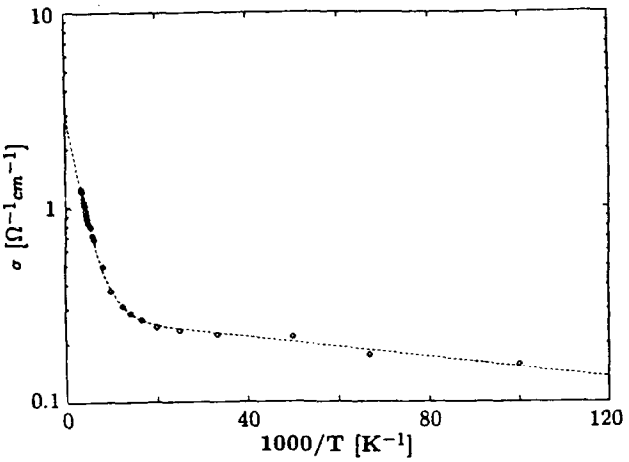

FIG. 1. Conductivity of GaN as a function of $1000/T$.

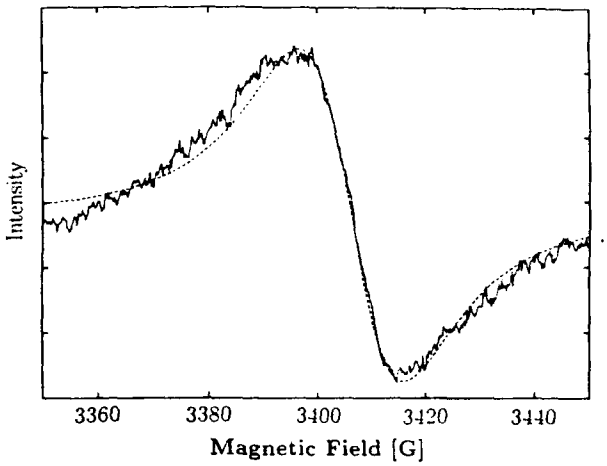

FIG. 2. First derivative absorption resonance line at 10 K and Lorentzian best fit.

lets, a result which we attribute to phase separation of excess gallium, presumably due to the narrow existence phase diagram of GaN. On the contrary, films produced under high nitrogen overpressure have carrier concentration between 10^{18}–10^{13} cm^{-3} and their surface is free of gallium droplets. This trend is consistent with the formation of nitrogen vacancies during growth and, if their concentration is very high, some gallium is phase separated in order for the material to maintain the stoichiometry allowed by its phase diagram. The samples investigated in this paper were free of any gallium droplets. Additionally, there is also theoretical support that the nitrogen vacancy in GaN is a shallow donor. Tight-binding calculations by Jenkins and Dow[8] have shown that the neutral unrelaxed N vacancy is a shallow donor with its singly occupied p-like level (T_2) in the conduction band and its doubly occupied s-like level (A_1) in the band gap close to the conduction-band edge. It is anticipated that lattice relaxation should shift the singly occupied level in the energy gap.

ESR measurements were performed at different temperatures in a Varian E9 spectrometer at 9.3 GHz, 100-kHz modulation frequency, and 0.5–1.0-G modulation amplitude. An α,α'-diphenyl-β-picrylhydrazyl reference was used to evaluate the g value. Figure 2 shows the ESR spectrum at 10 K of the same sample discussed in Fig. 1. This resonance has an isotropic g value of 1.9533 ± 0.0008 independent of temperature. The shape of the line is Lorentzian and the peak-to-peak linewidth ($\Delta H_{pp}=18\pm1$ G at 10 K) has a temperature dependence shown in Fig. 3. The broadening of the line with the increase in temperature prevented us from observing the resonance at temperatures higher than 110 K. The temperature dependence of the electron-paramagnetic-resonance (EPR) intensity is shown in Fig. 4.

From the saturation behavior of the resonance we estimated a spin-lattice relaxation time, at 10 K, of $(6\pm2)\times10^{-5}$ sec. No ESR signal was observed in semi-insulating GaN films.

To discuss the nature of the observed resonance we should first rule out that such a signal is not due to either plasma resonance or cyclotron resonance. Plasma resonance is ruled out based on the prediction of Dresselhaus,

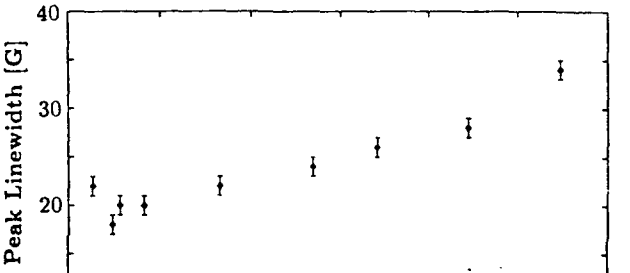

FIG. 3. Peak to peak linewidth ΔH_{pp} as a function of temperature.

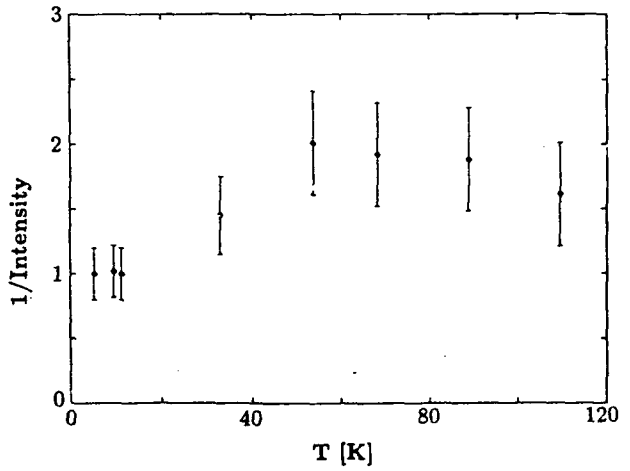

FIG. 4. Intensity of the EPR signal as a function of temperature (normalized to the value obtained at 5 K).

Kip, and Kittel[9] that the resonance moves to lower magnetic field as the frequency is increased. To test this we varied the microwave frequency in our experiment from 9.3 to 9.5 GHz and observed that the resonance moved to higher magnetic field instead. Electron cyclotron resonance also is ruled out since, assuming an effective mass similar to that of wurtzite GaN ($m^*/m_0=0.20\pm0.02$) (Ref. 10) the resonance should occur at a magnetic field ~ 5 times smaller than it was actually observed; moreover, a mobility three orders of magnitude larger than the value reported in similarly prepared GaN films[6] would be required to obtain a distinctive signal in the X band.

The observed resonance is therefore related to the ESR signal whose origin is due either to deep localized defects (intrinsic or impurities), or to delocalized electrons due to the shallow donors discussed earlier. However, the temperature dependence of the EPR intensity, shown in Fig. 4, does not follow the Curie-Weiss law suggesting that the electrons responsible for the observed resonance are not localized in deep defects. Additional arguments in favor of this conclusion are the lack of hyperfine or superhyperfine structure, expected for localized electrons in intrinsic defects of III-V semiconductors, and the lack of ESR signal in highly resistive films. The observed temperature dependence of the resonance intensity is not consistent with either a Curie or a Pauli paramagnetism. We can only speculate that the observed intermediate regime is related to the fact that the concentration of carriers in the band of the shallow donors as well as in the conduction band depend on temperature.

These findings, together with the conductivity data, suggest that the observed EPR signal at temperatures less than 50 K is due to delocalized electrons in the band of the previously discussed shallow donors and at temperatures higher than 50 K to electrons thermally activated into the conduction band. The fact that we did not observe a change in the g value as a function of temperature suggests that, to within the experimental accuracy, the g value is the same in both bands.

It is interesting to compare our experimental result of the electron g value with theoretical predictions based on the five-band model $\mathbf{k}\cdot\mathbf{p}$ calculation[11-14] and estimate the electron effective mass. According to this model the g value and the electron effective mass are given by the expressions

$$\frac{g^*}{g_e}-1=-\frac{P^2}{3}\left[\frac{\Delta_0}{E_0(E_0+\Delta_0)}+\lambda^2\frac{\Delta_0'}{(E_0'-E_0)(E_0'-E_0-\Delta_0')}\right], \tag{2}$$

$$\frac{m_0}{m^*}-1=\frac{P^2}{3}\left[\frac{3E_0+2\Delta_0}{E_0(E_0+\Delta_0)}-\lambda^2\frac{3(E_0'-E_0)-2\Delta_0'}{(E_0'-E_0)(E_0'-E_0-\Delta_0')}\right], \tag{3}$$

where $\Delta_0=\Gamma_{8v}-\Gamma_{7v}$, $\Delta_0'=\Gamma_{8c}-\Gamma_{7c}$, $E_0'=\Gamma_{8c}-\Gamma_{8v}$, and according to Chadi, Clark, and Burnham[13]

$$\lambda^2P^2=\frac{2}{m_0}|\langle\Gamma_{1c}|p_x|\Gamma_{5c,x}\rangle|^2, \tag{4}$$

$$P^2=\frac{2}{m_0}|\langle\Gamma_{1c}|p_x|\Gamma_{5v,x}\rangle|^2. \tag{5}$$

Hermann and Weisbuch[14] presented an estimate of P^2 based on simplified linear combination of atomic orbitals,

$$P_{\rm est}^2=\frac{\hbar^2\eta^2}{a^2m_0}\left[\frac{(1-\alpha_p^2)^{1/2}-S}{2(1-S^2)}\right]^2, \tag{6}$$

where α_p is the polarity and S is the overlap term[15] and η is a best-fit parameter $\eta=(1.04\pm0.07)\times10^3$.[14] From this expression, with $\alpha_p=0.62$ (Ref. 15) and $S=0.5$,[14] one obtains for GaN $P_{\rm est}^2=28\pm2$ eV. With the following values $E_0=3.2$ eV, $\Delta_0=0.009$–0.016 eV,[16] $\Delta_0'=0.06$–0.1 eV,[17] $E_0'=8.7\pm0.3$ eV,[18] $\lambda^2=0.4$,[13] we obtained $g^*=1.95\pm0.01$ in agreement with our experimental result. The electron effective-mass calculation yields a value of $m^*/m_0=0.15\pm0.01$, a value close to that measured experimentally for GaN films having the wurtzite structure [$m^*/m_0=0.20\pm0.02$ (Ref. 10)].

A brief comment on the utilized values for Δ_0, S, and λ^2 is necessary in order to put the previous calculation in the right perspective. Since the number and orientation of nearest and next-nearest neighbors are the same in the wurtzite and in the zinc-blende structures, the value of the spin-orbit splitting Δ_0 for zinc-blende GaN should not be significantly different from the value evaluated for the wurtzite structure. The latter is known[16] and used in our calculation. The overlap integral S and the parameter λ^2 depend primarily on the ionicity of the bond. GaN is the most ionic of the III-V compounds; however, its ionicity is close to the value for InP for which researchers have used $S=0.5$ (Ref. 14) and $\lambda^2=0.4$.[13]

The possible interaction mechanisms responsible for the spin-lattice relaxation rates of conduction electrons have been discussed by several authors.[19-21] As pointed out by Yafet[21] the dominant relaxation process, at least at not too low temperatures where the spin-current interaction should dominate, is the phonon modulation of the spin-orbit coupling. This mechanism gives the following spin-lattice relaxation rate:[21]

$$T_{1e}^{-1}\sim\frac{\lambda}{\pi^{3/2}\hbar}\frac{D^2}{\rho u^2}\left[\frac{2m^*kT}{\hbar^2}\right]^{5/2}, \tag{7}$$

where ρ is the density, u the sound velocity, and, for a polar semiconductor, $D\sim Cf\delta g(\hbar^2/am^*E_0)$ with C being the deformation potential, f the relative strength of the crystal potential that is odd under inversion, δg the g shift, a a parameter of the order of the lattice constant, and E_0 the optical gap. Using values appropriate to cubic GaN [$\rho=6.1$ g cm^{-3}, $u=6.9\times10^3$ msec^{-1}, $C\sim13$ eV,[22] $f=1$ (Ref. 11)] we find $T_{1e}\sim9\times10^{-5}$ sec at 10 K in general agreement with our experimental result.

In the effort to qualitatively account for the data of Fig. 3 we need to discuss spin-spin relaxation mechanisms which determine T_{2e} and thus the magnitude of the linewidth ΔH_{pp}. The analysis of the matrix elements which contribute to T_{2e}^{-1}, for the relaxation mechanism

previously discussed, show the same **k** and **q** dependence as the matrix elements used for T_{1e}^{-1}. Therefore, T_1, and T_{2e} have the same temperature dependence.[21] However Eq. (7) would predict a difference in the linewidths at 10 and 100 K by a factor ≈ 300, in contrast with the experimental results of Fig. 4. We believe that this disagreement is due to the fact that additional spin-spin relaxation mechanisms set in at low temperatures. One relevant relaxation mechanism at low temperatures is the hopping of electrons from one site to another. Such a process was observed to be the dominant line-broadening mechanism at low temperatures in heavily doped *n*-type silicon.[23] Our conductivity data have indicated hopping conduction, in the investigated sample at temperatures below 50 K, with an activation energy $\varepsilon_3 = 0.5$ meV due to overlap of the shallow donor wave functions and the presence of compensating defects.[7] In the case of hopping motion of electrons, the linewidth is inversely proportional to the probability p of the phonon-assisted transition from one center to another, $\Delta H_{pp} \propto 1/p$. This probability depends on temperature as[7,24]

$$p \propto \left[\exp\left[\frac{\varepsilon_3}{kT}\right]-1\right]^{-1}. \tag{8}$$

Therefore, at low temperatures, where hopping is the dominant broadening mechanism, one should observe an increase in the linewidth as the temperature decreases, as perhaps suggested by our experimental point at 5 K.

III. CONCLUSIONS

In conclusion, we reported the observation of an electron spin resonance in zinc-blende gallium nitride thin films produced by the electron-cyclotron-resonance microwave-plasma-assisted MBE method. The EPR signal was attributed to electrons predominantly in the band of autodoping centers (N vacancies) at low temperatures and in the conduction band at higher temperatures. The electron g value was found to be 1.9533 ± 0.0008. Using a five-band model and appropriate parameters for GaN a g value $g^* = 1.95 \pm 0.01$ in agreement with the experimental value was obtained and an effective mass $m^*/m_0 = 0.15 \pm 0.01$ was calculated.

From the saturation behavior of the resonance line a spin-lattice relaxation time of the order of 10^{-5} sec at 10 K was estimated in general agreement with the theoretical value predicted considering the phonon modulation of the spin-orbit interaction as the relaxation mechanism. The temperature dependence of the resonance linewidth was semiqualitatively accounted considering, besides the phonon modulation of the spin-orbit interaction, the hopping process at low temperature as an additional spin-spin relaxation mechanism.

ACKNOWLEDGMENTS

This research was supported by the Office of Naval Research (Grant No. N00014-92-J-1436). We are indebted to Professor Hans Van Willigen of the University of Massachusetts for the use of the ESR facilities.

[1] J. I. Pankove, H. P. Maruska, and J. E. Berkeyheiser, Appl. Phys. Lett. **5**, 197 (1970).
[2] J. I. Pankove, in *Diamond, Silicon Carbide, and Related Wide Bandgap Semiconductors*, edited by J. T. Glass, R. F. Messier, and N. Fujimori, MRS Symposia Proceedings No. 162 (Materials Research Society, Pittsburgh, 1990), p. 515.
[3] T. Lei, M. Fanciulli, R. Molnar, T. D. Moustakas, R. J. Graham, and J. Scanlon, Appl. Phys. Lett. **58**, 944 (1991).
[4] T. Lei, T. D. Moustakas, R. J. Graham, Y. He, and S. Berkowitz, J. Appl. Phys. **71**, 4933 (1992).
[5] J. I. Pankove, S. Bloom, and G. Harbeke, RCA Rev. **36**, 163 (1975).
[6] R. J. Molnar, T. Lei, and T. D. Moustakas, Appl. Phys. Lett. **62**, 72 (1993).
[7] N. F. Mott and W. D. Twose, Adv. Phys. **10**, 107 (1961).
[8] D. W. Jenkins and J. D. Dow, Phys. Rev. B **39**, 3317 (1989).
[9] G. Dresselhaus, A. F. Kip, and C. Kittel, Phys. Rev. **100**, 618 (1955).
[10] A. S. Barker and M. Ilegems, Phys. Rev. B **7**, 743 (1973).
[11] M. Cardona, *Semiconductors and Semimetals* (Academic, New York, 1967), Vol. 3, p. 125.
[12] L. M. Roth, B. Lax, and S. Zwerdling, Phys. Rev. **114**, 90 (1959).
[13] D. J. Chadi, A. H. Clark, and R. D. Burnham, Phys. Rev. B **13**, 4466 (1976).
[14] C. Hermann and C. Weisbuch, Phys. Rev. B **15**, 823 (1977).
[15] W. A. Harrison and S. Ciraci, Phys. Rev. B **10**, 1516 (1974).
[16] R. Dingle, D. D. Sell, S. E. Stokowki, and M. Ilegems, Phys. Rev. B **4**, 1211 (1971).
[17] Estimated from the general trend of other Ga-V compounds, close to GaP (Ref. 11) [D. J. Chadi (private communication)].
[18] S. Bloom, G. Harbeke, E. Meier, and I. B. Ortenburger, Phys. Status. Solidi **66**, 161 (1974).
[19] A. W. Overhauser, Phys. Rev. **89**, 689 (1953).
[20] R. J. Elliott, Phys. Rev. **96**, 266 (1954).
[21] Y. Yafet, in *Solid State Physics*, edited by F. Seitz and D. Turnbull (Academic, New York, 1963), Vol. 14.
[22] Estimated from the general trend of other semiconductors.
[23] B. G. Zhurkin, N. A. Penin, and P. Swarup, Fiz. Tverd. Tela (Leningrad) **8**, 3550 (1966) [Sov. Phys. Solid State **8**, 2839 (1966)].
[24] A. Miller and E. Abrahams, Phys. Rev. **120**, 745 (1960).

Appendix B:

Intensity dependence of photoluminescence in GaN thin films

Published in *Appl. Phys. Lett.* **64**, 336 (1994).

Intensity dependence of photoluminescence in GaN thin films

R. Singh, R. J. Molnar, M. S. Ünlü, and T. D. Moustakas
Molecular Beam Epitaxy Laboratory, Department of Electrical, Computer, and Systems Engineering, Boston University, Boston, Massachusetts 02215

(Received 30 August 1993; accepted for publication 15 November 1993)

We report the intensity dependence of band-gap and midgap photoluminescence in GaN films grown by electron cyclotron resonance (ECR) microwave plasma-assisted molecular beam epitaxy. We find that the band-gap luminescence depends linearly while the midgap luminescence has a nonlinear dependence on the incident light intensity. These data were compared with a simple recombination model which assumes a density of recombination centers 2.2 eV below the conduction band edge. The concentration of these centers is higher in films grown at higher microwave power in the ECR plasma.

Gallium nitride (GaN) is a wide direct band-gap semiconductor ($E_g = 3.4$ eV at 300 K), which is currently being investigated in many laboratories for its potential in optical devices (light emitting diodes, lasers, detectors) operating in the blue-violet ultraviolet part of the electromagnetic spectrum.[1] The performance and reliability of such devices depends critically on the type and concentration of electronic defects, whose origin is the heteroepitaxial growth (misfit dislocations and polarity related defects), the formation of native defects (vacancies, interstitials, and antisite defects) and the incorporation of intentional and unintentional impurities.

Defects in semiconductors can be studied by a variety of techniques, principal among which is photoluminescence (PL), a method which has been used extensively for the study of GaN films.[2,3] Photoluminescence spectra of undoped GaN films generally show a sharp peak close to the energy gap of the semiconductor, attributed to excitons bound to shallow donors[3] and a broader peak centered around 2.2 eV.[4,5] Various models have been advanced to account for the high shallow donor concentration in unintentionally doped GaN. The prevailing view is that the donors are due to nitrogen vacancies[6] although there is some evidence that oxygen impurities can also act as substitutional donors.[7] The broad yellow luminescence was attributed to electron transitions from the conduction band to a band of deep acceptor states placed 860 meV above the valence band edge.[8] These authors presented arguments that such states are introduced by carbon impurities in the films while Pankove *et al.*,[4] who observed the same photoluminescence band in ion implanted GaN samples, attributed the deep states to ion implantation processes. In general, the existence and magnitude of the yellow luminescence is associated with defective GaN films and the ratio of the yellow luminescence peak to band-gap luminescence was employed as a criterion of the carbon doping effects on the films[8] or the ion implantation related damage.[4]

In this letter, we investigated the excitation intensity dependence of PL from undoped GaN films and found that the band-gap luminescence depends linearly while the yellow luminescence has a nonlinear dependence on the light intensity. Thus the use of the ratio of yellow to band-gap luminescence as a criterion of the quality of the GaN films is meaningless unless one specifies the magnitude of the employed excitation light intensity. A simple recombination model has been proposed to qualitatively account for the observed light intensity dependence of the two luminescence bands.

The GaN films used in this study were grown by the electron cyclotron resonance microwave plasma-assisted molecular beam epitaxy (ECR-MBE), which was described in detail in a number of recent papers.[9,10] Here, we present only a brief description of the growth process. All the films were deposited on (0001) sapphire substrates, whose surface after chemical cleaning and thermal outgassing, is converted to AlN by exposing it to an ECR activated nitrogen plasma.[9] The films were deposited by the two-step growth process in which a GaN buffer of about 300 Å thick is deposited at 500 °C and the rest of the film, 1 to 2 μm thick, is deposited at 800 °C. This two-step growth method was found to lead to a low two-dimensional nucleation rate and a high lateral growth rate leading to films with relatively smooth surface morphology.[9,10] Power in the ECR discharge was the main variable during the growth of the films reported in this letter. More specifically type I samples were grown at a total microwave power of 20 W while type II samples were grown at 35 W. The transport coefficients of two representative samples are shown in Table I.

The photoluminescence was excited by a pulsed N_2 laser as the excitation source. The laser has a photon energy of 3.678 eV (337.1 nm), pulse, width of 10 ns, repetition rate of 40 Hz and a listed peak power of 250 kW. A circular aperture was used in front of the rectangular collimated beam and the resulting output was focused on the sample using a lens. A set of neutral density filters was used to attenuate the incident laser intensity for studying the excitation dependence of PL from the sample. The sample was held on a cold finger with a colloidal suspension of graphite which also acts as a

TABLE I. Typical values for the room temperature carrier concentration and mobility for representative type I and type II samples.

Sample	Power (W)	Carrier conc. (cm^{-3})	Mobility ($cm^2 V^{-1} s^{-1}$)
Type I	20	1.0×10^{18}	50
Type II	35	1.90×10^{17}	13.8

 0003-6951/94/64(3)/336/3/$6.00

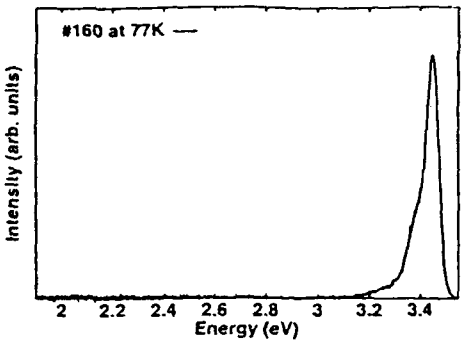

FIG. 1. PL spectra from a type I sample.

good heat conductor, hence preventing the sample from being heated by the laser. PL was collected by a lens and focused on the entrance slits of a 0.25-m grating spectrometer. A Hamamatsu photomultiplier (R-928) was used as the detector and its output was read by a lock-in amplifier. The spectra were not corrected for the spectral response of the system.

Figure 1 shows the photoluminescence spectrum at 77 K for a type I GaN sample. This spectrum shows only the band-gap luminescence at 3.47 eV. At the maximum excitation intensity we see no evidence of yellow luminescence, suggesting that the concentration of midgap defects is very low. The band-gap luminescence was found to vary linearly with light intensity over two orders of magnitude, a result consistent with excitonic recombination.[11]

The photoluminescence spectra of a type II GaN sample measured at 100% and 1% of the incident laser light is shown in Fig. 2. It is apparent from these data that characterizing the quality of the material by the ratio of the magnitude of the band-gap luminescence to the midgap luminescence is not correct, since the ratio depends on the excitation intensity. Thus, it is quite important to take the excitation intensity into account when analyzing any PL spectra for this material.

Figure 3 illustrates the intensity dependence of the band-gap and midgap luminescence peaks of the type II GaN sample. The band-gap luminescence depends linearly on light intensity as for type I samples. However, the midgap luminescence was found to have a light intensity dependence

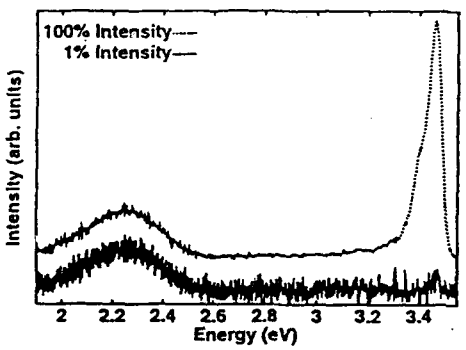

FIG. 2. PL spectra from type II samples at two different excitation levels.

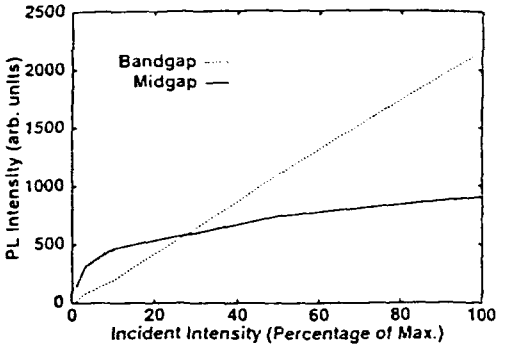

FIG. 3. Plot of the PL intensity vs the percentage excitation for the band-gap and midgap luminescence.

as shown in the figure. It initially increases with light intensity at low excitation levels and then tends to saturate as the excitation intensity is increased further.

The observed dependence on light intensity can be qualitatively accounted for in the simple recombination model illustrated in Fig. 4. We assume that the states responsible for the yellow luminescence form a broad band of a total density $N_{1\max}$. Shown in the figure are also the lifetimes for the various recombination paths and the densities N_1 and N_2 of the occupied states in the defect and conduction bands, respectively. If G ($\mathrm{cm^{-3}\,s^{-1}}$) is the generation rate then the rate of change of N_1 and N_2 are given by the equations

$$\frac{dN_2}{dt}=G-\frac{N_2}{\tau_{20}}-\frac{N_2}{\tau_{21}},\quad \frac{dN_1}{dt}=\frac{N_2}{\tau_{21}}-\frac{N_1}{\tau_{10}}. \tag{1}$$

Under steady-state conditions, i.e., when the recombination lifetimes are smaller or comparable to the duration of the excitation pulse, Eqs. (1) become

$$G=\frac{N_2}{\tau_{20}}+\frac{N_2}{\tau_{21}},\quad \frac{N_2}{\tau_{21}}=\frac{N_1}{\tau_{10}}. \tag{2}$$

The band-gap luminescence (I_{gap}) and the midgap luminescence (I_{yel}) are given by the expressions:

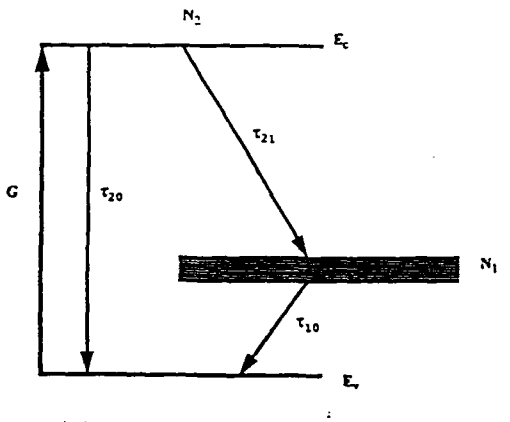

FIG. 4. Schematic of the proposed recombination model.

$$I_{gap} \propto \frac{N_2}{\tau_{20}} = \frac{G\tau_{21}}{(\tau_{21}+\tau_{20})}, \quad I_{yel} \propto \frac{N_2}{\tau_{21}} = \frac{G\tau_{20}}{(\tau_{21}+\tau_{20})}. \tag{3}$$

We assume that the recombination lifetimes τ_{20} and τ_{10} are constants while τ_{21} depends on light intensity. More specifically the value of τ_{21} can be expressed in terms of the low light intensity recombination lifetime τ'_{21} as[11]

$$\tau_{21} = \frac{N_{1max}}{N_{1max}-N_1}\,\tau'_{21}. \tag{4}$$

From Eqs. (3) and (4) we get

$$I_{gap} \propto \frac{GN_{1max}\tau'_{21}}{N_{1max}\tau'_{21}+(N_{1max}-N_1)\tau_{20}},$$
$$I_{yel} \propto \frac{G\tau_{20}(N_{1max}-N_1)}{N_{1max}\tau'_{21}+\tau_{20}(N_{1max}-N_1)}. \tag{5}$$

Case I: Low light intensity, i.e., $N_1 \ll N_{1max}$

$$I_{gap} \propto \frac{G\tau'_{21}}{\tau_{20}+\tau'_{21}}, \quad I_{yel} \propto \frac{G\tau_{20}}{\tau_{20}+\tau'_{21}}. \tag{6}$$

Hence, in this case the yellow and the band-gap luminescence increase proportionally to the incident light intensity.

Case II: High light intensity, i.e., $N_1 \cong N_{1max}$, the first of Eqs. (5) gives

$$I_{gap} \propto G. \tag{7a}$$

On the other hand, the yellow luminescence is governed by the recombination time, τ_{10}. Thus from Eqs. (2) and (3),

$$I_{yel} \propto \frac{N_{1max}}{\tau_{10}} \rightarrow \text{Const.} \tag{7b}$$

Equations (6) and (7) account qualitatively for the experimental results for Fig. 3.

Although this model does not take into account the change in the number of traps and recombination centers due to the shift in the quasi-Fermi levels as excitation intensity is changed,[12] it is sufficient to explain the saturation of the yellow PL from GaN. It would help further to have information about the recombination lifetimes of carriers to compute the exact number of midgap states.

In conclusion, we have determined the light intensity dependence of the band-gap and midgap luminescence in GaN films grown by electron cyclotron resonance assisted molecular beam epitaxy. As expected the band-gap luminescence varies linearly with the light intensity but the midgap luminescence initially increases and then saturates at higher light intensities. The data show the importance of relating I_{yel}/I_{gap} to the generation rate employed during the measurement for the purposes of comparing samples on the basis of PL spectra. It further illustrates that samples grown at higher microwave power have higher concentration of midgap defects, which accounts for the observed compensation in the transport coefficients.

This work was supported by the Office of Naval Research (Grant No. N00014-92-J-1436).

[1] S. Strite and H. Morkoç, J. Vac. Sci. Technol. B 10, 1237 (1992).
[2] J. I. Pankove, J. E. Berkeyheiser, H. P. Maruska, and J. Wittke, Solid State Commun. 8, 1051 (1970).
[3] R. Dingle and M. Ilegems, Solid State Commun. 9, 175 (1971).
[4] J. I. Pankove and J. A. Hutchby, J. Appl. Phys. 47, 5387 (1976).
[5] I. Akasaki and H. Amano, SPIE 1361, 138 (1990).
[6] J. I. Pankove, Mater. Res. Soc. Symp. Proc. 162, 515 (1990).
[7] W. Wiefert, R. Fanzhelal, E. Butter, H. Sobotta, and V. Riede, Cryst. Res. Technol. 18, 383 (1993).
[8] T. Ogino and M. Aoki, Jpn. J. Appl. Phys. 19, 2395 (1980).
[9] T. D. Moustakas, T. Lei, and R. J. Molnar, Physica B 36, 185 (1993).
[10] T. D. Moustakas and R. J. Molnar, Mater. Res. Soc. Proc. 281, 753 (1993).
[11] J. I. Pankove, *Optical Processes in Semiconductors* (Dover, New York, 1975).
[12] A. Rose, *Concepts in Photoconductivity and Allied Problems* (Wiley, New York, 1963), Number 19.

Appendix C:

Microstructures of GaN Films Deposited on (001) and (111) Si Using ECR-MBE

Submitted to *J. Mater. Res.*

Microstructures of GaN Films Deposited on (001) and (111) Si Using ECR-MBE

S. N. Basu
Department of Manufacturing Engineering, Boston University, Boston, MA 02215.

T. Lei and T. D. Moustakas
Molecular Beam Epitaxy Laboratory, Department of Electrical Engineering, Boston University, Boston, MA 02215.

ABSTRACT

The microstructures of GaN films, grown on (001) and (111) Si substrates, by a two-step method using ECR-MBE, were studied by electron microscopy techniques. Films grown on (001) Si had a predominantly zinc-blende structure. The GaN buffer layer, grown in the first deposition step accommodated the 17% lattice mismatch between the film and substrate by a combination of misoriented domains and misfit dislocations. Beyond the buffer layer, the film consisted of highly oriented domains separated by inversion domain boundaries, with a substantial decrease in the defect density away from the interface. The majority of defects in the film were stacking faults, microtwins and localized regions having the wurtzitic structure. The structure of the GaN films grown on (111) Si was found to be primarily wurtzitic, with a substantial fraction of twinned zinc-blende phase. Occasional wurtzitic grains, misoriented by a 30° twist along the [0001] axis were also observed.

INTRODUCTION

GaN films are currently being investigated in a number of laboratories due to their potential for applications in opto-electronic devices as well as high temperature and high frequency electronics.[1] These applications require the successful growth of high-quality crystals of GaN which can be intentionally doped *n*- and *p*-type.

Due to the lack of a native substrate, GaN has been grown heteroepitaxially on a variety of substrates by a number of vapor-phase methods.[2-4] Such heteroepitaxial growth leads to defects due to the differences in the lattice constant, thermal expansion coefficient and polarity between the substrate and film. Recently, significant improvements in the quality of heteroepitaxially grown GaN films have been achieved by using AlN[5] and GaN[6,7] buffers, which promote lateral growth, improving the surface morphology as well as the optical and electronic properties of the films.

The thermodynamically stable phase of this material is α-GaN, which has the HCP wurtzitic structure. However, epitaxial stabilization of β-GaN, having the FCC zinc-blende structure, has been recently achieved on a number of substrates with cubic symmetry, including β-SiC[8], (001) MgO[9], (001) GaAs[10] and (001) Si[11]. The epitaxial stabilization of β-GaN implies that the cohesive energy of wurtzitic and zinc-blende GaN are comparable.

In this paper, we report a comprehensive TEM study of the microstructures of GaN films on (001) and (111) Si substrates, deposited by the Electron Cyclotron Resonance assisted - Molecular Beam Epitaxy (ECR-MBE) method. A comprehensive x-ray diffraction study of both films as well as a preliminary TEM study of the films on (001) Si have been recently reported elsewhere.[11,12] The x-ray diffraction study examined both in-plane and out-of-plane orientations and concluded that the two polymorphs of GaN often coexist in the same film.

EXPERIMENTAL DETAILS

The details of the thin film growth have been reported elsewhere.[4,11] Briefly, the GaN films were grown on (001) and (111) Si substrates by the ECR-MBE method, using a Varian Gen-II MBE unit with an AsTeX model-1000 ECR source. Gallium was evaporated using a conventional Knudsen effusion cell, while molecular nitrogen was passed through the ECR source to produce atomic and ionic nitrogen. The films were deposited in two steps, which separated the nucleation and growth processes. Initially, a 300Å buffer layer of GaN was deposited at 400°C, followed by the deposition of the rest of the film at 600°C.

The surface morphology of the films were examined using a JOEL JSM 6100 scanning electron microscope (SEM) equipped with a Kevex detector with a Be window for energy dispersive x-ray spectroscopy (EDS). The samples were also examined in *plan-view and cross-section using a* Phillips CM-30ST transmission electron microscope (TEM) having a point-to-point resolution of 0.19 nm at 300 kV acceleration voltage. The plan-view samples were thinned to perforation from the substrate side only, leading to TEM observations of the top regions of the films.

RESULTS AND DISCUSSION

GaN Films on (001) Si

Figure 1a is a SEM micrograph of the surface of a GaN film grown on (001) Si showing a tile-like morphology. It has been previously reported that the edges of the 'tiles' are oriented along the <110> directions, presumably due to the lower surface energy of {110} surfaces due to a lower number of broken bonds.[11] Figure 2a shows a brightfield TEM micrograph of the film in cross-section. The buffer layer is marked in the figure. It

appears that the film has a columnar morphology. However, the diffraction pattern of the film and substrate, shown in figure 2b, confirms the epitaxial growth of GaN in the zinc-blende structure, in spite of the substantial lattice mismatch of 17%. The film actually consists of highly oriented domains. The diffraction pattern also confirms that the structure is cubic (zinc-blende). Although the wurtzitic phase of GaN has a lower energy, the zinc-blende structure is stabilized by the cubic symmetry of the substrate surface. The lattice parameter of GaN was measured to be 4.5Å, in agreement with previous reports.[8,10,11]

Another interesting feature is the presence of pits in the Si at the Si/GaN buffer interface, one of which is marked by an arrow in figure 2a. These pits are crystallographic, with the side walls corresponding to {111} planes. These pits have been observed previously in (001) Si substrates on which SiC films were deposited[13] and occur due to vacancy aggregation resulting from the diffusion of Si into the buffer layer along the {111} planes.

Figure 2a shows that certain domains are highly faulted while others are relatively fault free. The faults also lead to streaking in the diffraction pattern perpendicular to the fault planes. Figure 3 is a higher magnification micrograph showing two domains (marked as A and B). While A is faulted throughout the thickness of the film, B is relatively fault free towards the top. The two domains are separated by a boundary marked by arrows. Such boundaries have been previously reported in similar zinc-blende structures and have been identified as inversion domain boundaries (IDB).[14-16] These boundaries arise during impingement of two nuclei, that start with a Ga and N layer respectively, causing bonding between like atoms across the boundary. Thus, the tile-like morphology, evident in figure 1a consists of highly oriented domains, separated by {110} inversion domain boundaries.

In general, the domains are highly faulted near the interface, with the fault density decreasing away from the interface. Figure 4 is a high resolution TEM micrograph of an

upper region of a domain showing the various types of faults in the film. The majority of the faults away from the interface are along the {111} planes and can be identified as stacking faults (marked as S), microtwins (marked as T) and hexagonal regions (marked as H). Such faults are known to occur in FCC materials having a low stacking fault energy.[17] Since there is evidence that the cohesive energies of the two polymorphs of GaN are comparable, the formation energy of the stacking faults in this material should be small.[18] It has been previously suggested that the wurtzitic structure is nucleated preferentially at stacking faults and twin boundaries of the zinc-blende structure in isostructural InN[19] and SiC.[20]

Figure 5 is a high resolution TEM micrograph of the buffer region in cross section. The figure shows the buffer layer to be highly faulted and polycrystalline, which is expected since this is where the lattice mismatch is accommodated. The inset diffraction pattern shows texturing along the [001] direction with a substantial number of misoriented grains. The grains in the buffer layer also exhibit a substantially larger density of stacking faults, leading to localized regions of wurtzitic structure (marked as H) and twins (marked as T) in figure 5. The interface between the buffer layer and the Si substrate appears to be disordered. This has been reported previously,[8,10] and can be attributed to a combination of damage during specimen preparation and a larger amount of disorder arising from the relatively large mismatch between the two lattices. The interfacial structure is visible in select areas, one of which, marked by a circle in figure 5, is shown at a higher magnification. Periodic interfacial misfit dislocations can be clearly identified in the figure. It thus appears that the misfit is accommodated in the buffer layer by a combination of misoriented grains and misfit dislocations.

The misoriented grains in the buffer layer are cut off by the oriented (001) domains away from the interface. As an example, one misoriented grain, marked as A in

figure 5, is close to the (111) orientation. Since, the (111) grain grows more slowly than the (001) domains, it is buried in the interface region as the film grows. Figure 5 clearly shows that the film deposited in the second stage above the buffer layer is highly oriented, with a substantial decrease in the fault density.

GaN Films on (111) Si

Figure 1b shows the surface of the GaN film grown on (111) Si. The tile-like morphology of the GaN film on (001) Si is no longer evident. Figure 6 shows a plan-view brightfield TEM micrograph of the film. The figure shows the presence of domains, which are highly oriented as seen by the inset diffraction pattern. X-ray diffraction analysis showed the film to be primarily wurtzitic with a substantial fraction of zinc-blende structure.[11,12] It should be noted, however, that this diffraction pattern cannot distinguish between the two phases. These domains are separated by boundaries which have been identified as inversion domain boundaries as well as stacking faults arising from the impingement of two GaN domains that are rotated by 60° around the [0001] axis. Sitar et al. have named these boundaries as double positioning boundaries (DPB) and have observed them in α-GaN films on (0001) sapphire, SiC and ZnO substrates.[21] Double positioning boundaries have also been studied in cubic β-SiC films on (0001) 6H-SiC substrates.[17,22] A more detailed analysis of the faults at the boundaries will be presented elsewhere.[23]

Figure 6 shows the presence of stacking faults in certain grains marked by arrows. Stacking faults in α-GaN leads to localized regions of zinc-blende structure in the film. Figure 7 shows a darkfield micrograph taken using only a cubic reflection, indicating the distribution of the zinc-blende structure in the GaN film. This appears to be consistent with the estimate of 25% cubic phase by x-ray diffraction analysis.[12,18] This observation has

significant implications for the optical and electronic properties of such films. The optical gap of wurtzitic GaN is 3.4 eV while that of cubic GaN is 3.2 eV.[1,11] The incorporation of 25% of the zinc-blende phase in the wurtzitic structure should affect the optical gap as well as the transport and recombination phenomena in these films. Figure 8 shows that the zinc-blende phase appears to be concentrated within certain domains and not randomly distributed throughout the film.

Figure 8a is a brightfield micrograph of the GaN film grown on (111) Si in cross-section. The figure also shows the columnar morphology of the domains. Figure 8b shows the diffraction pattern obtained from the film and substrate. Figure 8c shows the indexed pattern (except for some double diffraction spots) showing the presence of the wurtzitic (marked as H) and zinc-blende (marked as C) phases as well as the twinned variant of the cubic zinc-blende structure (marked as T). The orientation relationships as seen from the diffraction pattern are as follows:

$(111)Si \parallel (111)\beta\text{-GaN} \parallel (0002)\alpha\text{-GaN}$ and $[\bar{1}\,10]Si \parallel [\bar{1}\,10]\beta\text{-GaN} \parallel [11\bar{2}\,0]\alpha\text{-GaN}$.

This orientation allows the alignment of the closest packed planes and directions of all three phases. The presence of a substantial fraction of zinc-blende structure is not surprising due to the identical symmetry of the (0002) and (111) planes in the wurtzitic and zinc-blende structures respectively, along with the small difference in the cohesive energy of the two polytypes.

Another interesting feature of these film was the presence of occasional wurtzitic grains that were misoriented by a 30° twist along the [0001] axis with the rest of the wurtzitic grains. Figures 9a and 9b show a brightfield TEM micrograph of such a grain and the corresponding diffraction pattern. Figure 10c is a darkfield micrograph highlighting the misoriented grain. Figure 10 shows the atomic positions at an

unreconstructed interface between the misoriented GaN grain and the (111) Si substrate. The coincident (or near coincident) atomic positions are marked by circles. The figure shows that every fourth N (or Ga) atom is in position to directly bond with every third Si atom at the interface. This boundary would thus have a lower energy than a random boundary and could explain the presence of these misoriented GaN grains. This is an example of a near coincidence boundary between two phases, discussed by Ballufi et al.[24], where Σ_N (=4) $\neq$ Σ_{Si} (=3), due to the difference in the planar atomic densities of the two phases. A hexagonal supercell formed between the two phases is marked by bold lines in the figure and has a lattice parameter of 6.5Å.

CONCLUSIONS

The microstructures of GaN films, grown by a two-step method using ECR-MBE on (001) and (111) Si, was studied using electron microscopy techniques. The structure of films grown on (001) Si was found to be predominantly zinc-blende. The GaN buffer layer, grown in the first deposition step was found to be highly faulted, and accommodated the strain due to lattice mismatch between the substrate and film by a combination of misoriented domains and misfit dislocations. Beyond the buffer layer, the film consisted of highly oriented domains separated by inversion domain boundaries. There was a substantial decrease in the defect density away from the interface, with the majority being defects in the stacking sequence along the {111} planes, leading to stacking faults, microtwins and localized regions having the wurtzitic structure.

The structure of the GaN films grown on (111) Si was found to be primarily wurtzitic. However, a substantial fraction of twinned zinc-blend structure was also identified in the films. The rest of film consisted of highly oriented wurtzite domains

separated by inversion domain and stacking faults. Occasional wurtzitic grains, misoriented by a 30° twist along the [0001] axis were also observed in the film.

ACKNOWLEDGMENTS

Dr. T.E. Mitchell and Dr. K. Das Chowdhury are gratefully acknowledged for stimulating discussions. The authors would also like to thank Anlee Kruup for her help with the SEM analysis and Dhruv Bhatt and Christopher McDowell for their help with TEM specimen preparation. TEM studies were carried out at the Center for Materials Science at Los Alamos National Laboratory. A portion of this work was sponsored by the Office of Naval Research (Grant # N00014-92-J-1436).

REFERENCES

1. R. F. Davis, Proceedings of the IEEE **79**, 702 (1991).

2. H. P. Maruska and J. J. Tietjen, Appl. Phys. Lett. **15**, 327 (1969).

3. H. M. Manasevit, F. M. Erdmann and W. I. Simpson, J. Electrochem. Soc. **118**, 1864 (1971).

4. T. D. Moustakas, T. Lei and R. J. Molnar, Physica B **185**, 36 (1993).

5. H. Amano, N. Sawaski, I. Akasaki and y. Toyoda, Appl. Phys. Lett. **48**, 353 (1986).

6. T. Lei, M. Fanciulli, R. J. Molnar, T. D. Moustakas, R. J. Graham and J. Scanlon, Appl. Phys. Lett. **59**, 944 (1991).

7. S. Nakamura, Jpn. J. Appl. Phys. **30**, L1705 (1991).

8. M. J. Paisley, Z. Sitar, J. B. Posthill and R. F. Davis, J. Vac. Sci. Technol. A **7**, 701 (1989).

9. R. C. Powell, G. A. Tomasch, Y. W. Kim, J. A. Thorton and J. E. Greene, Mat. Res. Soc. Symp. Proc. **162**, 525 (1990).

10. S. Strite, J. Ruan, Z. Li, A. Salvador, H. Chen, D. J. Smith, W. J. Choyke and H. Morkoç, J. Vac. Sci. Technol. B **9** (4), 1924 (1991).

11. T. Lei, T. D. Moustakas, R. J. Graham, Y. He and S. J. Berkowitz, J. Appl. Phys. **71** (10), 4933 (1992).

74, 4430 (1993)

12. T. Lei, K. F. Ludwig and T. D. Moustakas, J. Appl. Phy. (Oct., 1993)

13. C. M. Chorey, A Transmission Electron Microscopy Study of β-Silicon Carbide Grown Epitaxially on Silicon, M.S. Thesis, Case Western Reserve University, Cleveland, OH (1987).

14. T. E. Mitchell, P. Pirouz and A. H. Heuer, Microbeam Analysis, R. H. Geiss, Ed., San Francisco Press, San Francisco, CA, 215 (1987).

15. A. Georgakilas, J. Stoemenos, K. Tsagaraki, Ph. Komninou, N. Flevaris, P. Panayotatos and A. Christou, J. Mater. Res. **8** (8), 1908 (1993).

16. R. F. Davis, J. W. Palmour and J. A. Edmond, Mat. Res. Soc. Symp. Proc. **162**, 463 (1990).

17. P. Pirouz and Y. Yang, Mat. Res. Soc. Symp. Proc. **183**, 173 (1990).

18. T. Lei and T. D. Moustakas, Mat. Res. Soc. Symp. Proc. **433**, 173 (1992).

19. S. Strite, D. Chandrasekhar, D. J. Smith, J. Sariel, H. Chen, N. Teraguchi and H. Morkoç, J. Cryst. Growth **127**, 204 (1993).

20. L. U. Ogbuji, T. E. Mitchell, A. H. Heuer and S. Shinozaki, J. Am. Cer. Soc. **64** (2), 100 (1981).

21. Z. Sitar, M. J. Paisley, B. Yan and R. F. Davis, Mat. Res. Soc. Symp. Proc. **162**, 537 (1990).

22. H. S. Hong, B. L. Jiang, J. T. Glass, G. A. Rozgonyi and K. L. More, J. Appl. Phys. **63** (8), 2645 (1988).

23. S. N. Basu, K. Das Chowdhury and T. D. Moustakas, manuscript under preparation.

24. R. W. Balluffi, A. Brokman and A. H. King, Acta Metall. **30**, 1453 (1982).

LIST OF FIGURE CAPTIONS

Figure 1. SEM micrographs of the surface of GaN film deposited on a) (001) Si and b) (111) Si.

Figure 2. a) TEM brightfield micrograph of GaN film grown on (001) Si in cross-section. The GaN buffer layer as well as the presence of pits in the Si are marked in the figure. b) Diffraction pattern of the interface showing the epitaxial orientation of zinc-blende GaN on (001) Si.

Figure 3. TEM brightfield micrograph of GaN film grown on (001) Si in cross-section, showing two domains marked as A and B, separated by an inversion domain boundary marked by arrows.

Figure 4. High resolution TEM micrograph of the upper region of GaN film grown on (001) Si, showing a stacking fault, marked as S; a microtwin, marked as T; and a hexagonal wurtzitic region marked as H.

Figure 5. High resolution TEM micrograph of the buffer region of GaN film grown on (001) Si. The inset diffraction pattern shows that although there is a (001) texturing in the buffer layer, there are a significant number of misoriented grains. The presence of wurtzitic regions and microtwins are marked by H and T respectively. Although the interface between the buffer and Si appears to be highly disordered, lattice planes can be seen up to the interface in a few areas, one of which is marked by a circle. A magnified micrograph of the marked region shows the presence of misfit dislocations at the interface.

Figure 6. Plan-view brightfield TEM micrograph of GaN film grown on (111) Si, showing the presence of domains. Grains with stacking faults are marked by arrows, indicating the presence of the cubic phase. The diffraction pattern shows that the film is highly oriented and has a hexagonal symmetry common to the (0002) and (111) planes of wurtzitic and zinc-blende structures.

Figure 7. Darkfield TEM micrograph of GaN film grown on (111) Si, using a cubic reflection, highlighting the zinc-blende phase in the material.

Figure 8. a) TEM brightfield micrograph of GaN film grown on (111) Si in cross-section, showing columnar morphology of the domains. b) Diffraction pattern of the interface. c) Indexed diffraction pattern showing presence of wurtzitic phase (H) as well as zinc-blende phase (C) that is twinned (T), along with the reflections from the Si substrate (Si).

Figure 9. a) TEM brightfield micrograph of a wurtzitic grain in GaN film grown on (111) Si. b) Selected area diffraction pattern, showing a 30° twist about the [0001] axis with respect to the surrounding grains. c) Darkfield micrograph highlighting the misoriented grain.

Figure 10. Interfacial structure of the misoriented grain/Si substrate. The coincident or near coincident atomic positions at the interface is marked by circles. A hexagonal supercell with a lattice parameter of 6.5Å is also marked by bold lines in the figure.

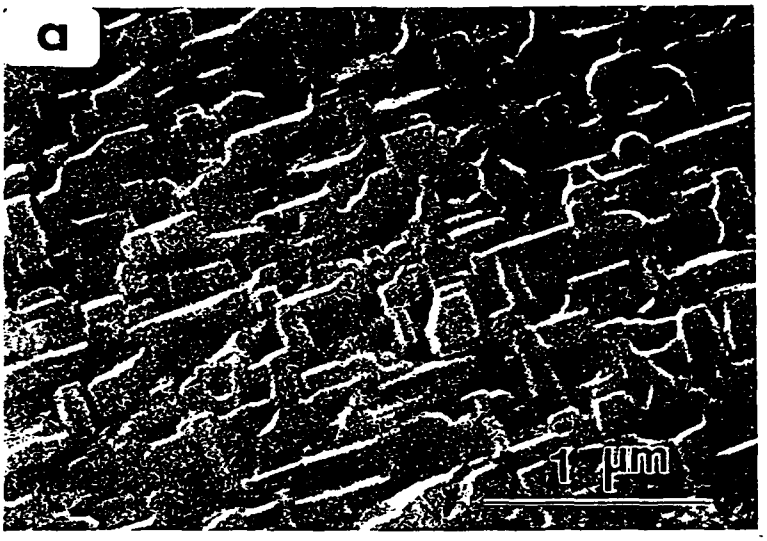

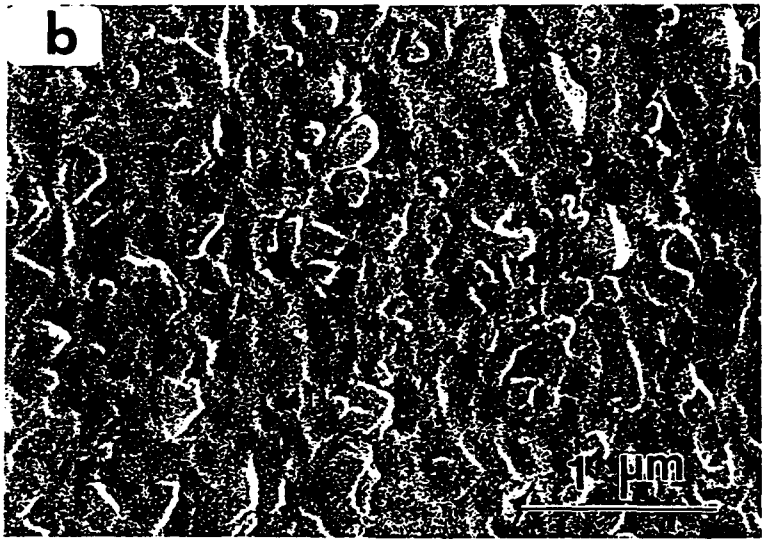

Fig. 1

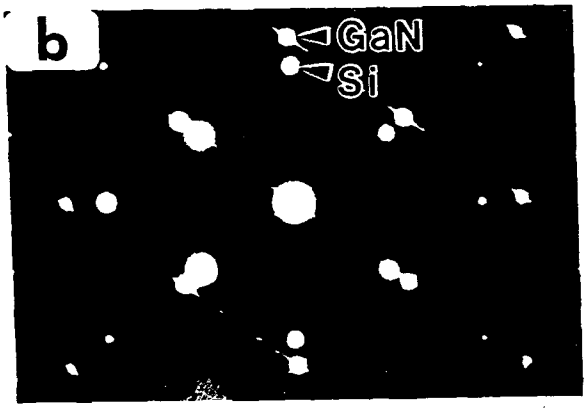

Fig2

F.93

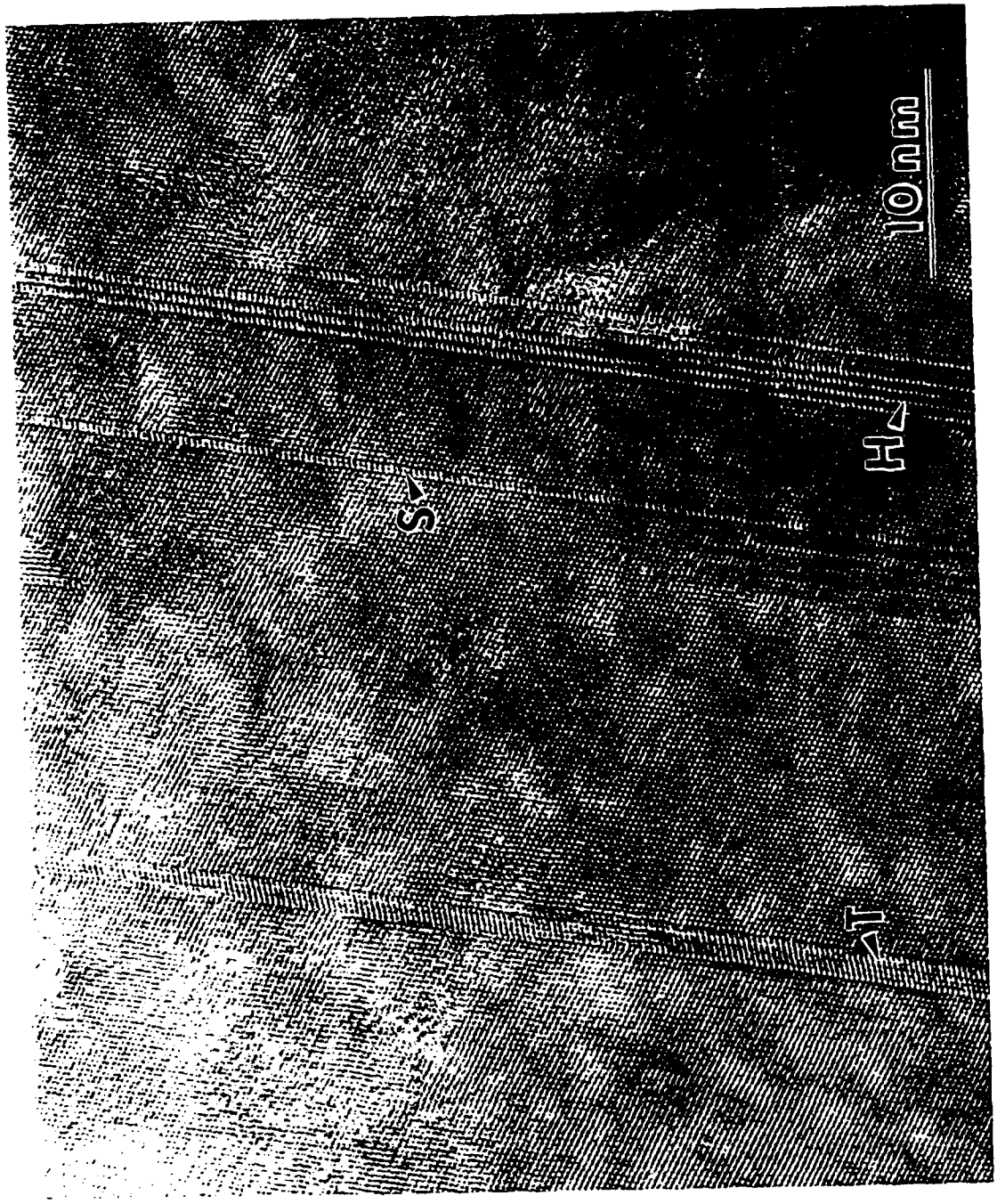

Fig. 4

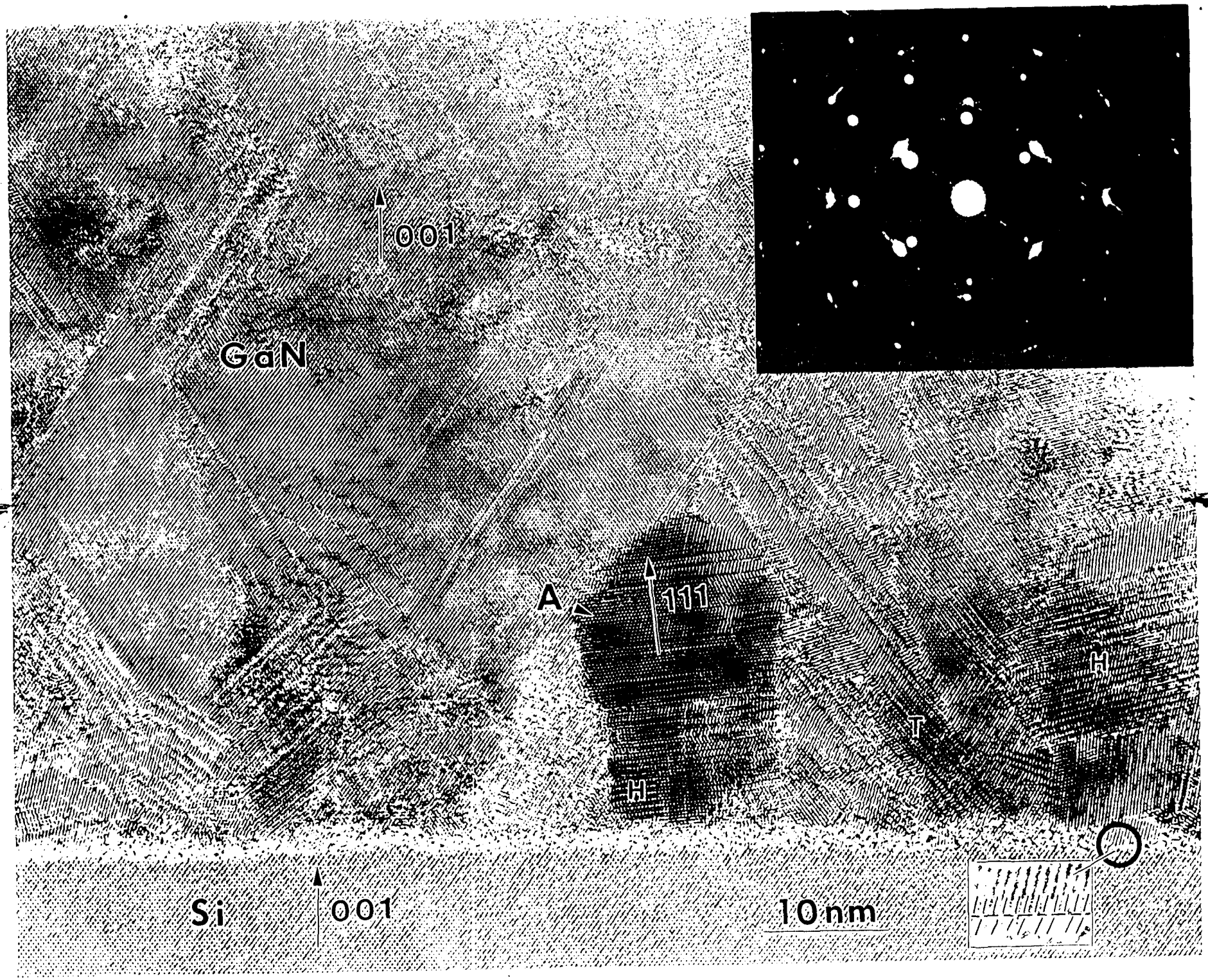
001
GaN
A
111
H
T
H
Si
001
10nm

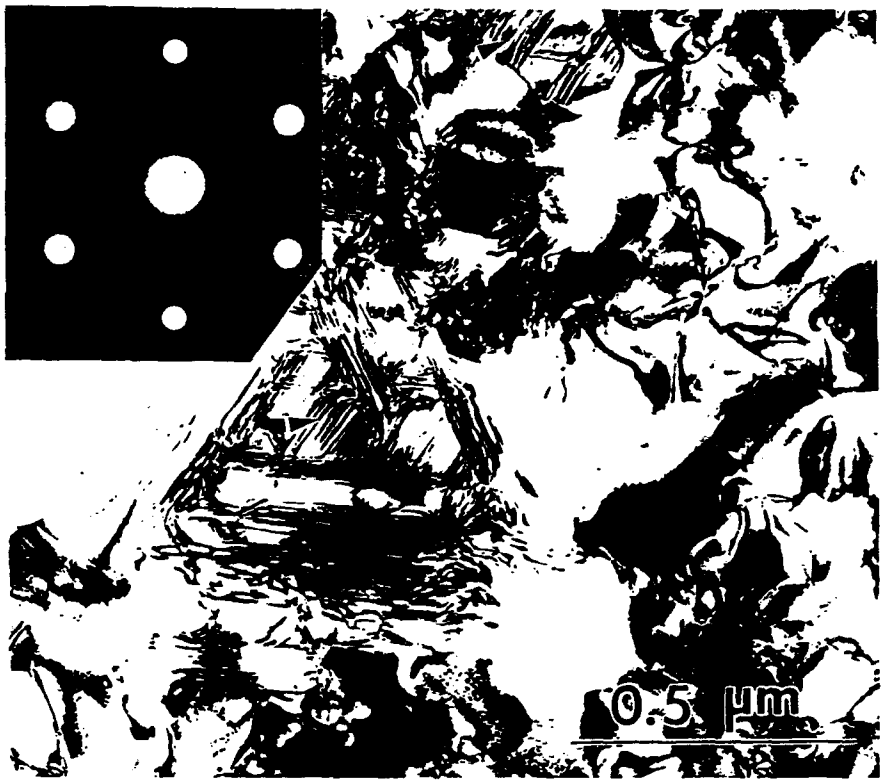

Fig.

Fig. 7

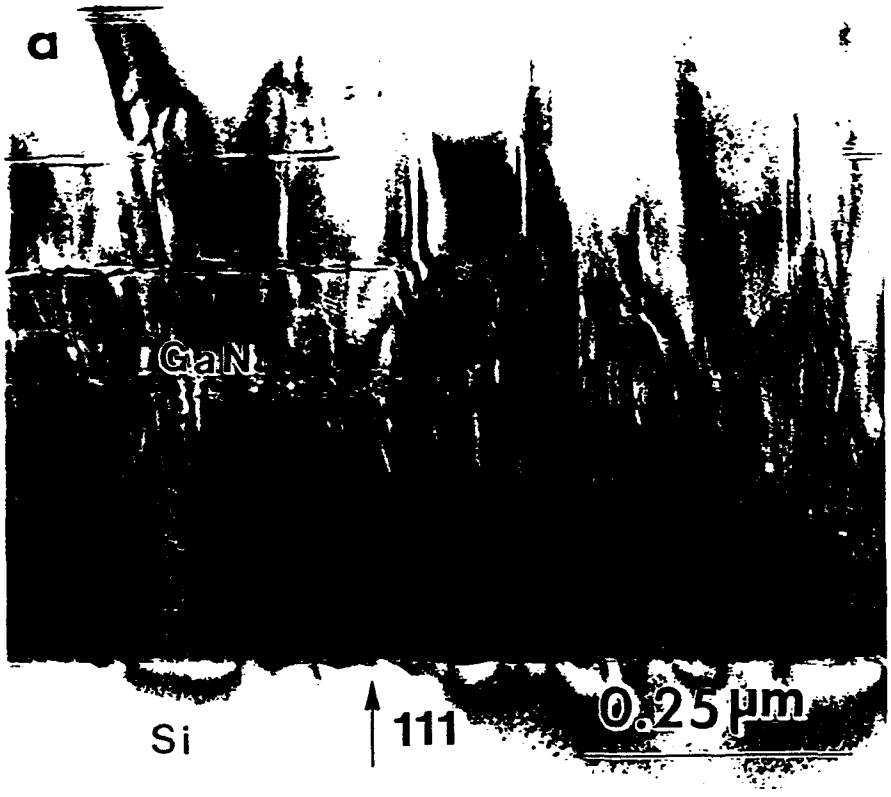
a
GaN
Si
111
0.25 μm

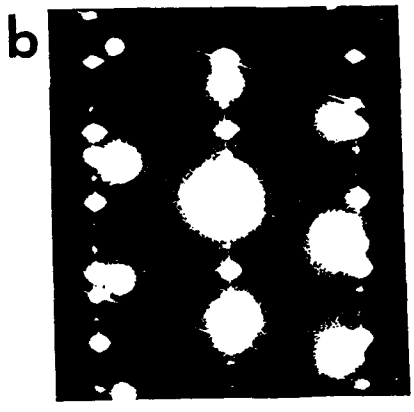
b

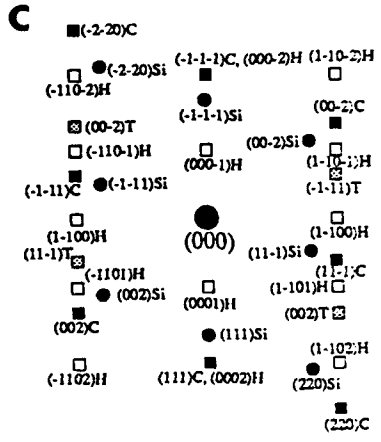
c
(-2-20)C
(-2-20)Si
(-110-2)H
(-1-1-1)C, (000-2)H
(1-10-2)H
(-1-1-1)Si
(00-2)C
(00-2)T
(-110-1)H
(00-2)Si
(000-1)H
(1-10-1)H
(-1-11)C
(-1-11)Si
(-1-11)T
(1-100)H
(000)
(1-100)H
(11-1)T
(11-1)Si
(-1101)H
(1-1-1)C
(002)Si
(0001)H
(1-101)H
(002)C
(002)T
(111)Si
(1-102)H
(-1102)H
(111)C, (0002)H
(220)Si
(220)C

Fig. 5

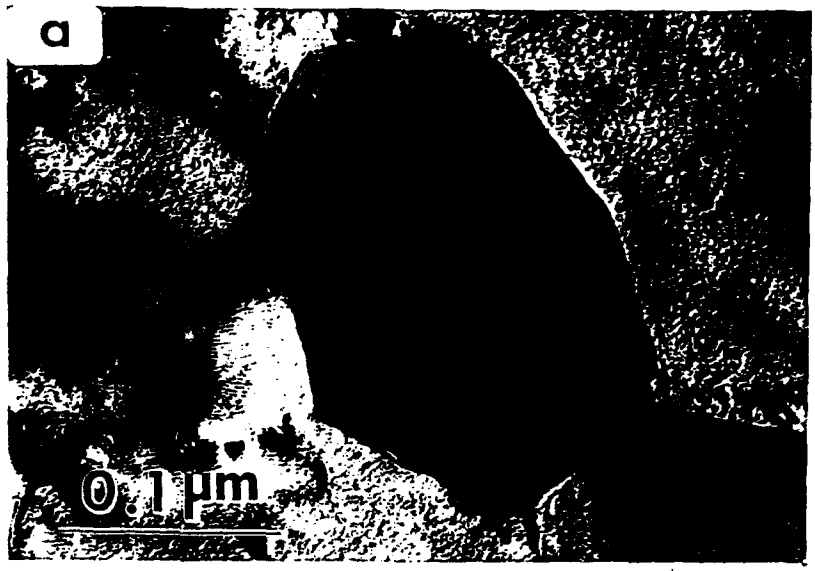

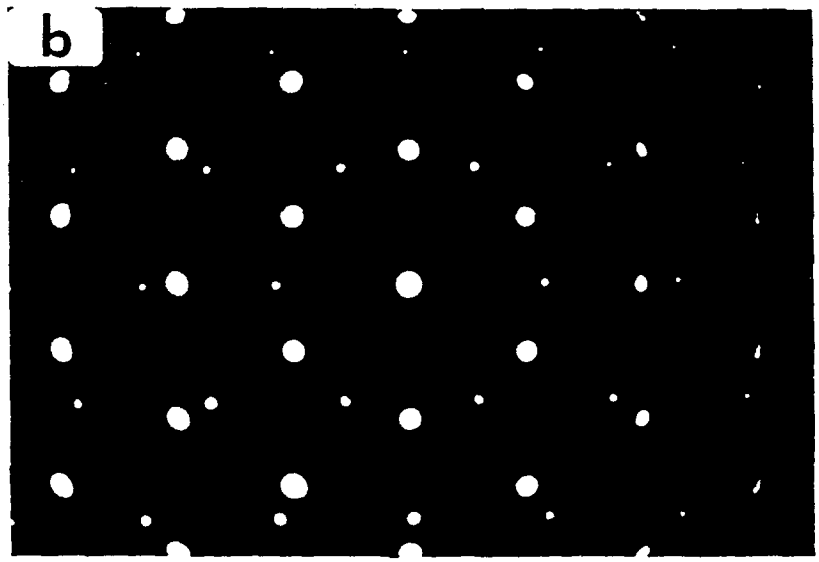

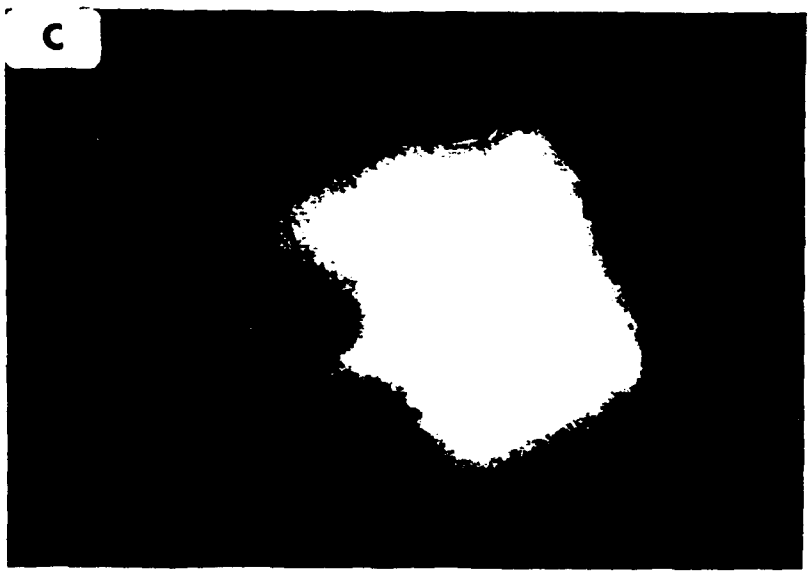

Figs

Appendix D:

Hydrogenation of Gallium Nitride
Accepted for Publication in *Material Research Society Proceedings* (1994).

HYDROGENATION OF GALLIUM NITRIDE

M. S. BRANDT,* N. M. JOHNSON,* R. J. MOLNAR,** R. SINGH,** AND T. D. MOUSTAKAS**

* Xerox Palo Alto Research Center, 3333 Coyote Hill Road, Palo Alto CA 94304
** Department of Electrical, Computer, and Systems Engineering, Boston University, Boston, MA 02215

ABSTRACT

A comparative study of the effects of hydrogen in n-type (unintentionally and Si-doped) as well as p-type (Mg-doped) MBE-grown GaN is presented. Hydrogenation above 500°C reduces the hole concentration at room temperature in the p-type material by one order of magnitude. Three different microscopic effects of hydrogen are suggested: Passivation of deep defects and of Mg-acceptors due to formation of hydrogen-related complexes and the introduction of a hydrogen-related donor state 100 meV below the conduction band edge.

INTRODUCTION

The effects of hydrogen on the electronic and vibrational properties of various semiconductors have been studied extensively [1]. In elemental semiconductors, one observes, e.g., the passivation of deep defects (dangling bonds) in amorphous silicon, resulting in a decrease of the subgap absorption, or the passivation of dopant atoms such as boron or phosphorous, resulting in a decrease of the carrier concentration. In recent years, these studies have been extended to compound semiconductors, but have been mostly restricted to the GaAs/AlAs system and InP. With respect to the possible effects of hydrogen wide-bandgap III-V and II-VI semiconductors like GaN and ZnSe have only recently received attention. This interest has been triggered by an intriguing difficulty to achieve p-type doping in films grown with one particular growth technique. In both the II-VI and III-V systems it is found that metal-organic chemical vapor deposition (MOCVD) is unable to produce p-type material, while molecular-beam epitaxy appears to easily grow p-type samples. This behaviour has been linked to the presence of hydrogen in the gas phase during MOCVD growth, which might lead to the formation of acceptor-hydrogen complexes. Indeed, in the case of N-doped p-type ZnSe, the observation of N-H local vibrational modes in MOCVD material strongly supports this assumption [2].

In this contribution, we report on continuing studies of the effects of hydrogen in both n-type (unintentionally doped, sometimes called autodoped, and Si-doped) and p-type (Mg-doped) GaN. In p-type samples grown by MOCVD, acceptor dopants have to be activated by either a low-energy electron beam irradiation or by a thermal annealing step [3]. Again, the formation of accceptor-hydrogen complexes under the abundant presence of hydrogen has been suggested as the origin for the necessity of a post-growth process. We therefore use MBE-grown GaN and deliberately introduce hydrogen by remote-plasma hydrogenation to study the effects of hydrogen in this III-V compound.

SAMPLE GROWTH AND ANALYTICAL PROCEEDURES

Wurtzite GaN epilayers were grown on (0001) sapphire substrates by ECR-assisted MBE [4]. Gallium and the dopant elements (Mg and, for intentional n-type doping, Si) were evaporated

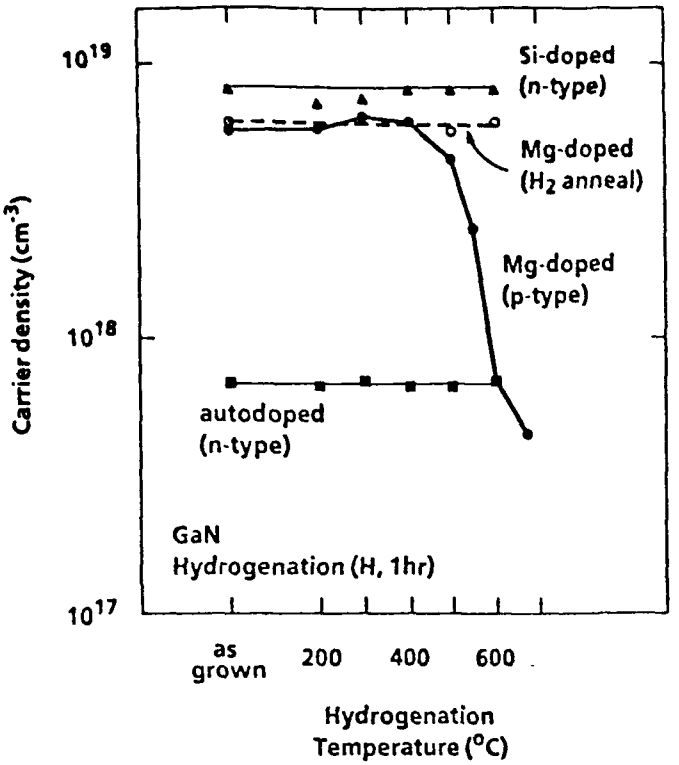

Figure 1: Dependence of the carrier concentration on hydrogenation temperature in epitaxial layers of GaN.

from conventional Knudsen cells, while nitrogen radicals were produced by passing molecular nitrogen through an ECR source at a pressure of 10^{-4} Torr. A microwave power of 35 W or higher was used for the growth of semi-insulating GaN films. Prior to the growth of the GaN epilayer, the substrates were exposed to the N-plasma for 30 min to form an AlN layer. A further GaN buffer layer was then grown at 500°C followed by the high-temperature growth of the actual film at 800°C at a growth rate of 200-250 nm/hr. Hydrogenation was performed with a remote microwave plasma operating at 2 Torr. This technique excludes effects due to charged particle bombardment of the sample or its illumination from the plasma. A high temperature sample holder allowed hydrogenation at temperatures up to 675°C. The films were electrically characterized in a standard Hall-effect apparatus, with the samples abrasively etched into a clover-leaf shape. For ohmic contacts Au was deposited on p-type GaN and Al on n-type material. Depth profiles were determined from secondary ion mass spectroscopy (SIMS), with a Cs^+ primary ion beam for the detection of hydrogen/deuterium and Si and an O^- primary beam for Mg. Calibration of the SIMS data was achieved with Mg and deuterium-implanted GaN reference samples. To increase the sensitivity, the GaN samples for SIMS were treated with a plasma containing deuterium instead of hydrogen. The photoluminescence measurements were performed with a pulsed N_2 laser as the excitation source (3.678 eV).

RESULTS

Figure 1 shows the carrier concentration at room temperature for three differently doped samples subjected to isochronal (1hr) hydrogenation. The n-type samples are completely uneffected by the hydrogenation, however the p-type sample shows a significant decrease in the hole concentration after hydrogenation at $T \geq 500$°C. The mobility in all three cases remained unchanged after hydrogenation at typically 50 cm^2/Vs (autodoped), 10 cm^2/Vs (Si-doped) and 0.3 cm^2/Vs (Mg-doped). A control experiment on the p-type sample is included in Fig. 1, where the microwave plasma was switched off during the post-growth treatment demonstrating that exposure

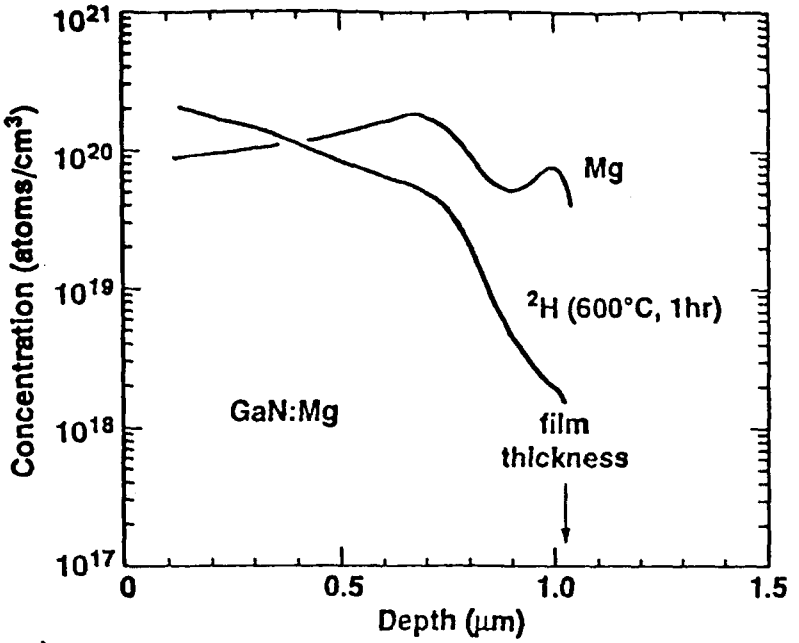

Figure 2: Depth profiles of hydrogen and magnesium in p-type GaN determined by SIMS.

to molecular hydrogen at temperatures up to 600°C does not affect the hole concentration.

Secondary-ion mass spectrosopy is used to verify the introduction of hydrogen into the material. In addition, together with the carrier concentrations determined in Fig. 1 the measurement of the dopant concentrations allows the determination of the doping efficiencies in Si- and Mg-doped GaN. Figure 2 shows the H- and Mg-depth profiled for p-type GaN. An average Mg-concentration of $10^{20}cm^{-3}$ is found, which indicates a very high doping efficieny of about 10%. The average hydrogen concentration is about the same as the Mg-concentration. The slight decrease in H-concentration up to a depth of $0.7\mu m$ could be due to a diffusion process. The steep decrease in the concentration, however, coincides with the doping inhomogeneity visible in the Mg-profile at $0.9\mu m$. The high Mg-concentration at the substrate interface might be due to outdiffusion of Mg from doped GaN layers deposited on the substrate holder during previous depositions.

A similar comparison of the dopant and deuterium depth profiles is given for Si-doped n-type GaN in Fig. 3. The average Si-concentration is about $4 \times 10^{20}cm^{-3}$, the doping efficiency of several percent is therefore slightly lower than in the p-type material. Two hydrogen profiles are included in Fig. 3. It becomes obvious that after hydrogenation at 600°C, the hydrogen concentration levels at $2 \times 10^{20}cm^{-3}$, independent of the local Si concentration, which is found to vary throughout the sample.

The hydrogen concentration, after the same passivation step, incorporated in the unintentionally (autodoped) material is about one order of magnitude lower than in Si-doped material (Fig. 4), and has a constant concentration profile. Comparing the hydrogen concentrations in the three differently doped samples we find that the hydrogen incorporation is not just limited by factors like solubility, but does indeed depend on the type and concentration of the dopant present.

Further information on the effects of hydrogen in GaN were obtained from photoluminescence (PL). In Fig. 5, a comparison is shown between the photoluminescence of Mg-doped and autodoped samples, both before and after hydrogenation at 600°C. The two dominant PL-lines in the as-grown samples are the exciton line at 3.41 eV and the Mg-acceptor related line at 3.25 eV, with its two phonon replicas. After hydrogenation, these lines are still observed in the respective samples, but a quantitative comparison of signal heights is difficult. In the autodoped sample, the hydrogenation led to a complete quenching of the defect related line at 2.3 eV [5]. In addition to these known PL lines, a new PL line at 3.35 eV appears after hydrogenation in both samples, which has not been previously reported in GaN.

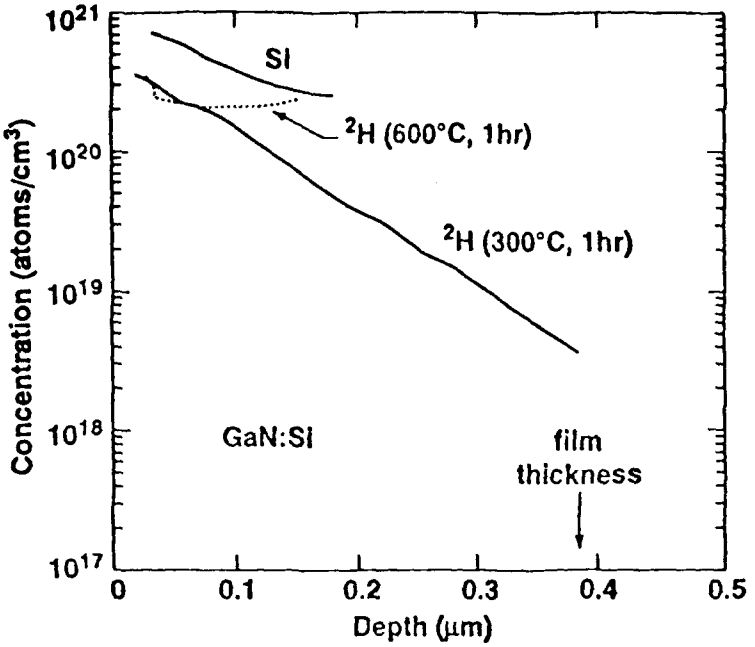

Figure 3: Depth profiles of hydrogen and silicon in n-type GaN determined by SIMS. The hydrogen profiles have been obtained on two identical samples treated at different passivation temperatures.

DISCUSSION

A similar hydrogen-related study on p-type GaN has already been performed by Nakamura and coworkers [6]. However, there are various significant differences to the results reported here. Nakamura used MOCVD grown samples, which were LEEBI-treated to obtain p-type conductivity. In our case, the MBE gown films are p-type without any need for a post-growth treatment. Nakamura used an NH_3 ambient for hydrogenation and had to rely on the thermal decomposition of the molecules on the surface of the film to obtain atomic hydrogen. Our experiments, in which the atomic hydrogen is produced in a remote plasma, therefore show that the hydrogenation temperature of 500°C is indeed typical for the material, and not just for the NH_3 cracking process. Details of the photoluminescence results also differ. Nakamura et al. saw an increase in a possibly defect-related PL band centerd at 1.65 eV after their ammoniation treatment. No indication for such a PL line is visible in our spectra. The remote hydrogen plasma used in our hydrogenation technique therefore does not lead to defect formation detectable in PL. In fact, the quenching of the defect-related line at 2.3 eV for the n-type sample (Fig. 5) shows that hydrogen can passivate this deep defect state, most probably by a complex formation process. We can conclude that in the experiments presented here, no compensation due to deep defect formation takes place. The observed changes in the hole concentration therefore appear to arise from compensation by shallow donor states created by the incorporation of hydrogen, or by a Mg-H complex formation.

A donor-like state related to the introduction of hydrogen would indeed be consistent with both the Hall data and the photoluminescence experiments. Under this assumption, the position of the new PL line 100 meV below bandgap would indicate the energy level of this new donor state. One has then to rationalize that the introduction of hydrogen into the n-type samples does not change the effective electron concentration, as visible in Fig. 1. The SIMS data reveal about 10^{19}cm^{-3} and 10^{20}cm^{-3} hydrogen in the autodoped and in the Si-doped samples, respectively, after hydrogenation, thereby giving an upper limit for the additional donor concentration in these samples. Only 1/100 of these would be thermally activated at room temperature, leading to an added electron concentration well below the Hall concentrations measured for these samples which would be difficult to detect.

The presence of Mg-H complexes, which would passivate the acceptors in contrast to compensation as discussed above, would be shown by the observation of a local vibrational mode of such

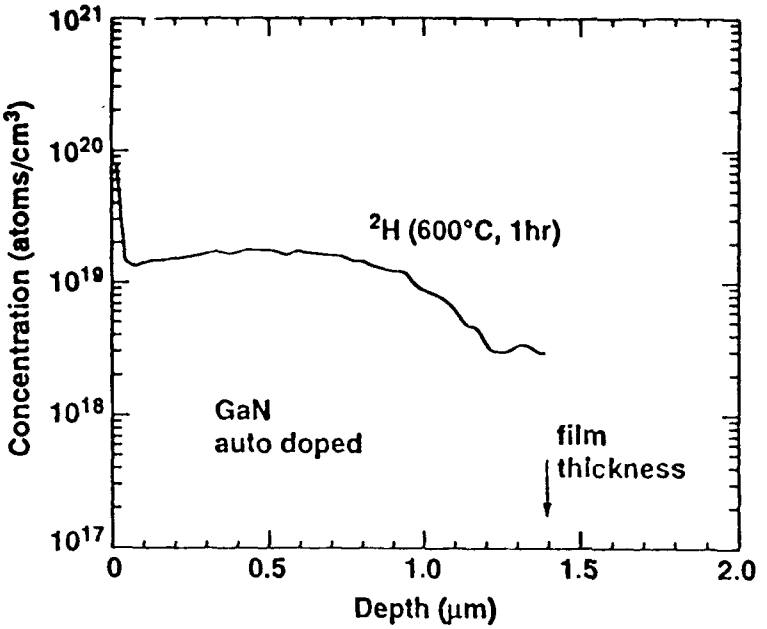

Figure 4: Depth profiles of hydrogen in unintentionally (autodoped) n-type GaN determined by SIMS.

a complex, as has been achieved for the N-H-complex in ZnSe. Preliminary Raman and infrared studies on the samples studied here indeed show such modes in the vicinity of 2200cm^{-1} when Mg concentrations above 10^{19}cm^{-3} are present in the samples [7]. No indication for Si-H, C-H and N-H vibrational modes has been found, however. Details of these results will be subject to a future publication.

The observation of both the new PL line in n- and p-type samples and of the LVM of Mg-H complexes in p-type material suggests that hydrogen can have various effects on the properties of GaN. Indeed, in the p-type sample one has to conclude from vibrational spectroscopy and the PL measurements that both effects, the compensation and the passivation, are present, although from the relative intensities of the PL line at 3.35 eV in the p-type and autodoped samples one might expect that the hydrogen-donor state concentration is small in the p-type material. However, the chemistry of hydrogen in GaN is clearly a challenging subject [8], which will require considerably more experimental and theoretical work.

SUMMARY

We have presented a comparative study of the effects of hydrogen in n- and p-type MBE-grown GaN. We find that the hole concentration in Mg-doped samples can be significantly reduced by hydrogenation above 500°C. The electron concentration in autodoped and Si-doped material is unaffected by hydrogenation. The observation of a new photoluminescence line at 3.35 eV in both n- and p-type samples suggests that hydrogen has a donor-like state in GaN. The defect-related PL line at 2.3 eV can be effectively quenched by hydrogenation, which indicates defect-hydrogen complex formation. As a third effect of hydrogen in GaN, Mg-H complexes are observed in vibrational spectroscopy.

ACKNOWLEGEMENTS

The authors are pleased to acknowledge J. Ager and W. Götz for the preliminary results from Raman spectroscopy and infrared absorption spectroscopy. They also thank C. Van de Walle

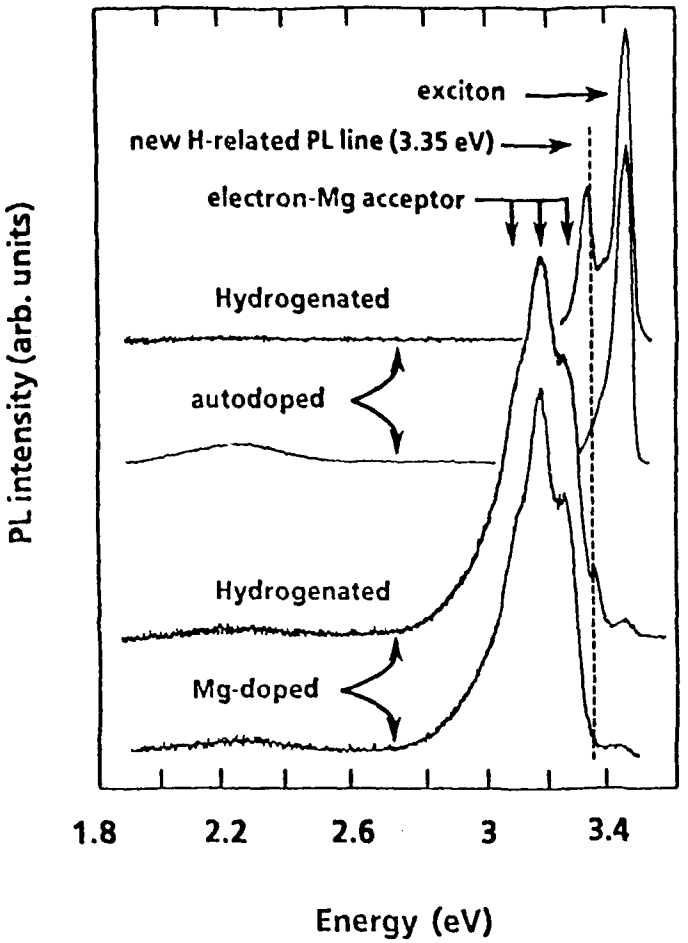

Figure 5: Photoluminescence spectra of autodoped and Mg-doped GaN, both before and after hydrogenation.

and E. E. Haller for helpful discussions and J. Walker and S. Ready for technical assistance. The work at Xerox was supported by AFOSR under contract F49620-91-C-0082 and at Boston University by ONR under contract N0014-92-j-1436. One of the authors (M.S.B.) acknowledges partial support from the Alexander von Humboldt-Stiftung.

REFERENCES

[1] *Hydrogen in Scmiconductors*, edited by J. I. Pankove and N. M. Johnson (Academic. San Diego, 1991).

[2] J. A. Wolk, J. W. Ager III, K. J. Duxstad, E. E. Haller, N. R. Taskar, D. R. Dorman, and D. J. Olego, Appl. Phys. Lett. **63**, 2756 (1993).

[3] H. Amano, M. Kito, K. Hiramatsu, and I. Akasaki, Jpn. J. Appl. Phys. **28**, L2112 (1989).

[4] T. D. Moustakas and R. J. Molnar, Mat. Res. Soc. Conf. Proc. **281**, 753 (1993).

[5] J. I. Pankove and J. A.Hutchby, J. Appl. Phys. **47**, 5387 (1976).

[6] S. Nakamura, T. Mukai, M. Senoh, and N. Iwasa, Jpn. J. Appl. Phys. **31**, L139 (1992), S. Nakamura, N. Iwasa, M. Senoh, and T. Mukai, Jpn. J. Appl. Phys. **31**. 1258 (1992).

[7] J. Ager and W. Götz, *private communication.*

[8] J. A. Van Vechten, J. D. Zook, R. D. Horning, and B. Goldenberg, Jpn. J. Appl. Phys. **31**, 3662 (1992).

Appendix E:

Reactive Ion Etching of GaN Thin Films
Accepted for Publication in *Material Research Society Proceedings* (1994).

REACTIVE ION ETCHING OF GaN THIN FILMS

Michael Manfra[1], Stuart Berkowitz[1], Richard Molnar[2], Anna Clark[1], T.D. Moustakas[2] and W.J. Skocpol[1]

[1]Department of Physics, Boston University, Boston Ma 02215
[2]Department of Engineering, Boston University, Boston Ma 02215

ABSTRACT

Reactive ion etching of GaN grown by electron-cyclotron-resonance, microwave plasma-assisted molecular beam epitaxy on (0001) sapphire substrates was investigated. A variety of reactive and inert gases such as CCl_2F_2, SF_6, CF_4, H_2/CH_4 mixtures, CF_3Br, CF_3Br/Argon mixtures and Ar were investigated. From these studies we conclude that of the halogen radicals investigated, Cl and Br etch GaN more effectively than F. The etching rate was found to increase with decreasing pressure at a constant cathode voltage, a result attributed to larger mean free path of the reactive species.

INTRODUCTION

The family of refractory nitrides (InN, GaN, AlN), their solid solutions and heterojunctions are one of the most promising families of electronic materials. All three binary compounds are direct bandgap semiconductors with energy gaps covering the region from 1.95eV (InN) and 3.4eV (GaN) to 6.28eV (AlN). These materials should find applications in optical devices (LED's lasers, detectors) operating in the green-blue-UV parts of the electromagnetic spectrum. Due to their unique physical properties, the materials are also expected to find applications in high temperature, high power, and high frequency electronic devices. However, the fabrication of such devices requires the development of a number of device processing techniques, including reactive ion etching.

There are limited reports in the literature regarding etching of GaN [1-4]. Pankove [1] reported that GaN dissolves in hot alkali solutions at very slow rates, and thus, wet etching is not practical for this strongly bonded material. Foresi [2] reported the reactive ion etching of GaN grown on the R-plane of

sapphire using CCl_2F_2, and Adesida [3] reported the etching of GaN using $SiCl_4$. Pearton [4] investigated ECR microwave discharges for the etching of GaN, InN and AlN.

In this paper we report on reactive ion etching studies of GaN grown on (0001) sapphire substrates using a variety of reactive and inert gases. The effect of plasma parameters on etch rate, morphology and selectivity were investigated.

EXPERIMENTAL METHODS

The GaN films were grown onto (0001) sapphire substrates by the method of electron-cyclotron-resonance microwave plasma-assisted molecular beam epitaxy (ECR-MBE) using a two temperature step growth process [5,6]. In this method a GaN buffer is grown first at low temperature (500°C) and the rest of the film is grown at higher temperatures. This process was shown [5,6] to lead to high lateral growth rate resulting in a layer by layer growth. The films have the wurtzite structure with the c-axis perpendicular to the substrate. Although the films were not intentionally doped they were found to be n-type with carrier concentrations in the order of $10^{18}cm^{-3}$, due presumably to nitrogen vacancies.

The ion etching of the GaN films was carried out in a parallel plate reactor supplied with 13.5 MHz RF power. Various patterns were formed on the top of the GaN films with AZ 1350 J photoresist. Various reactive and inert gases were employed. The depth of the profile of the etches was determined by a profilometer or by directly measuring the thickness by a cross-sectional SEM image. The quality of the etch morphology was also assessed by SEM imaging.

EXPERIMENTAL RESULTS AND DISCUSSION

First the etching rate from different reactive and inert gases was investigated. To compare the results the etching was carried out at the same gas pressure (11mT) and the same cathode voltage (600V). The results are listed in Table I.

Table I. Etching rates of GaN (11mT and 600V cathode voltage.)

Gas	Etching Rate (Å/min)
CCl_2F_2	185
CF_3Br	150
CF_3Br/Ar (3:1)	200
CF_4	120
SF_6	100
H_2/CH_4 (2:1)	30
Ar	65

From these results it is apparent that F is a less efficient etchant of GaN than the other halogen radicals Cl and Br. Etching by hydrogen radicals and physical sputtering are even less efficient processes. Nevertheless, the mixture of a certain percentage of Ar in CF_3Br improves the etching rate of the reactive gas.

The effect of gas pressure on the etching rate of GaN was investigated by using CF_3Br/Ar (3:1) and a constant cathode voltage of 600V. The results are shown in Figure 1.

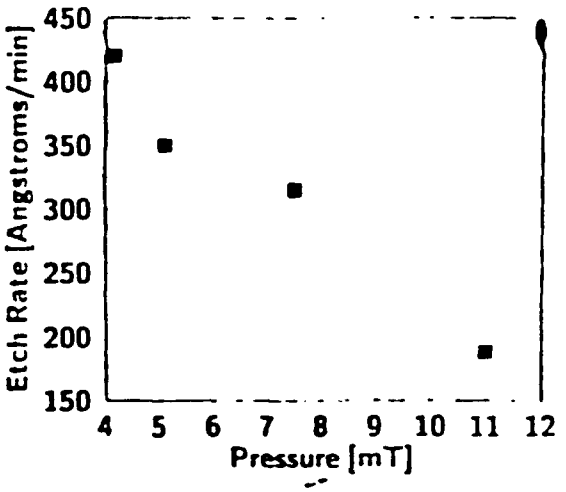

Fig. 1 Etch rate of GaN vs. the pressure of CF_3Br/Ar (3:1) at a constant cathode bias of 600V.

The higher etching rate at lower pressures suggests that the limiting step in the etching process is the mean free path of the halogen radicals. A typical etching profile obtained at 11mT of CF_3Br/Ar (3:1) and 600V of cathode voltage is shown in Figure 2.

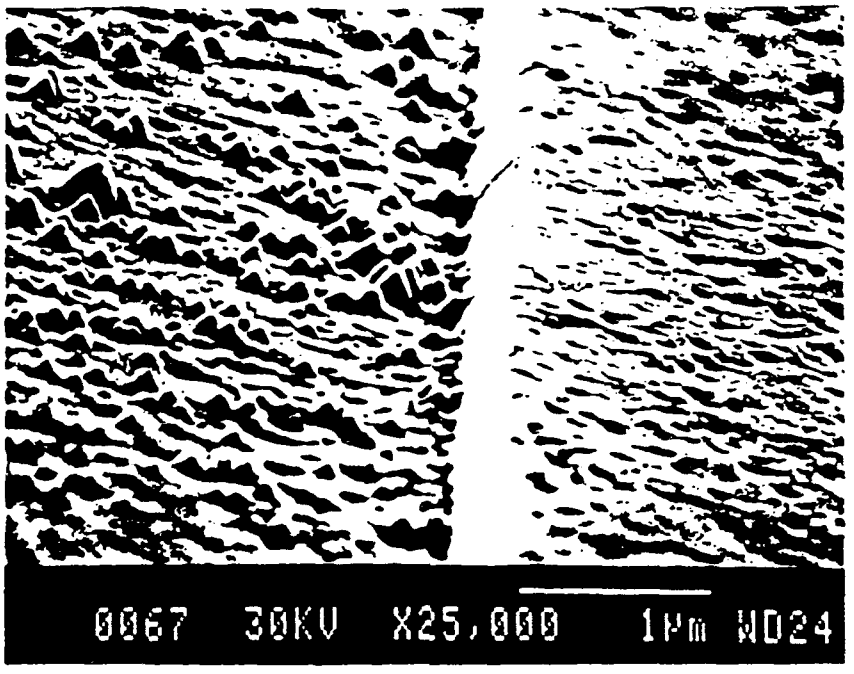

Fig. 2 A typical etch profile of GaN using CF_3Br/Ar (3:1) made under conditions described in the text.

We observed that the pyramidal features in the etching pattern are not present when etching was carried out at 5mT. By measuring the thickness of the photoresist prior to and after etching the selectivity at 5mT was found to be greater than 3:1 GaN to photoresist.

CONCLUSIONS

We report on reactive ion etching of GaN grown onto (0001) sapphire. Various reactive and inert gases were employed from which it was found

that Cl and Br etch GaN more effectively than F. The effects of plasma parameters on etch rate and surface morphology were investigated using a CF_3Br/Ar mixture in a 3:1 ratio. Etch rate and surface morphology were found to improve at lower plasma pressure, resulting in an etch rate in excess of 400 Å/min at 4.2 mT.

ACKNOWLEDGEMENTS

This work was supported by the Office of Naval Research (grant no. N00014-92-J 1436).

REFERENCES

1. J.I. Pankove, Electrochem. Soc. Vol **119**, 1110 (1972)

2. J. Foresi, M.S. Thesis (Boston University, 1991)

3. I. Adesida, A. Mahajan, E. Andideh, M. Asif Khan, D.T. Olsen and J.N. Kuzna Appl. Phy. Lett. **63**, 2777 (1993)

4. S.J. Pearton, C.P. Abernathy, F. Ren, J.R. Lothian, P.W. Wisk, A. Katz, and C. Constantine, Semicond. Sci. Technol. Vol 8 pg 310 (1993)

5. T.D. Moustakas, T. Lei and R. Molnar, Physica B 185 pg 36-49 (1993)

6. T.D. Moustakas and R. Molnar Mat. Res. Soc. Symp. Proc. Vol 281 (1993)